International Tables for Crystallography (2018). Vol. H, Chapter 3.9, pp. 344–373.

3.9. Quantitative phase analysis

I. C. Madsen, N. V. Y. Scarlett, R. Kleeberg and K. Knorr

3.9.1. Introduction

The field of quantitative phase analysis (QPA) from powder diffraction data is almost as old powder diffraction itself. Debye and Scherrer first developed the method around 1916 (Debye & Scherrer, 1916, 1917) and between 1917 and 1925 Hull (1917, 1919) and Navias (1925) were reporting studies of QPA related to the new technique. However, further developments in QPA were relatively slow, as much of the activity in X-ray diffraction (XRD) at the time was dedicated to the solution of crystal structures rather than the extraction of other information present in a powder diffraction pattern. While a small number of QPA applications continued to be published in the intervening years, it was not until the advent of scanning diffractometers around 1947 (Langford, 2004, Parrish, 1965) and the work of Alexander and Klug in 1948 (Alexander & Klug, 1948), which provided the formal methodology and a practical approach, that the field began to expand.

Since those original developments, which utilized the intensity of individual peaks or a small group of peaks in the diffraction pattern, there have been extensions to the methodology that use whole-pattern approaches. These methods operate *via* the summation of either (i) patterns collected from pure components or (ii) component contributions calculated from their crystal structures. There are a number of benefits accruing from the whole-pattern approaches since all reflections in the pattern, which may number in the hundreds or thousands, now contribute to the final analysis.

The mathematical basis of QPA is well established and, ideally, QPA should be a relatively straightforward science. However, there are a significant number of factors, many of them experimental, that serve to decrease the accuracy that can be obtained (Chung & Smith, 2000). Some of these, such as accuracy and precision in measurement of peak position and intensity, resolution of overlapping peaks and counting statistics, relate to instrument geometry and data-collection conditions. Other sources of error derive from sample-related issues and include effects such as (i) preferred orientation (which distorts the observed relative intensities from those expected for a randomly oriented powder); (ii) crystallite size and strain broadening (leading to increased peak width and hence overlap); (iii) the grain-size effect (where there may be too few crystallites contributing to the diffraction process to ensure that a representative powder pattern can be measured);[1] and (iv) microabsorption (where phases that strongly absorb the incident and diffracted beams are underestimated with respect to weakly absorbing phases). Of these, microabsorption remains the largest impediment to accurate QPA and is more pronounced in X-ray diffraction than in neutron-based studies.

While there is a very broad scope for the application of diffraction-based estimation of phase abundance, the perceived difficulty involved in developing and using these methods often deters non-specialist users. Consequently, they may resort to other, non-diffraction, material characterization techniques that are more readily implemented.

Analytical techniques for most of the 92 naturally occurring elements are generally well established and, in many cases, the subject of internationally accepted standards. However, the physical properties of minerals and materials formed by these elements, and the manner in which they react, is not solely dependent on their chemical composition but also on how the constituent elements are arranged; that is, their crystal structures. This finite number of known elements combines in an almost infinite array within the 230 crystallographic space groups. Further variability is induced by factors such as solid solution, degree of crystallinity and morphology, thus making QPA by diffraction methods considerably more difficult to implement.

In industry, many manufacturing or processing lines are controlled by measurement of elemental composition alone, simply because these values can be readily obtained to a high degree of accuracy and precision. For example, a plant extracting Cu from an ore body might measure the Cu content of the feed ore and the concentrate, and the plant conditions are optimized based on efficiency of extraction. However, if the mineralogical form of the Cu changes in the feed, then it may not behave in the same manner during grinding, flotation and density separation, and this will affect the recovery. Frequently, where knowledge of the mineralogy or phase abundance is actually used in plant optimization and control, it is derived from bulk or microcompositional analysis rather than being measured directly. This is often achieved by normative calculation, where the results of element composition analysis are assigned to specific phases based on an assumed knowledge of individual phase composition. Further details of this approach can be found in Chapter 7.7.

In materials science, new compounds are being synthesized at a rapidly increasing rate with techniques such as high-throughput synthesis capable of generating hundreds of new variants in a single experiment. Such techniques are being used in fields ranging from drug discovery, catalyst synthesis and new metal alloy design. The properties of these materials, and their suitability for their designed purpose, are not only dependent on their structural form but, for multiphase materials, on the amount of each component present. In this case, accurate, or at the very least reproducible, QPA is crucial to the screening process.

This chapter focuses on the application of QPA techniques for the extraction of phase abundance from diffraction data. While there is extensive coverage of the QPA methodology in other texts (Klug & Alexander, 1974; Smith *et al.*, 1987; Snyder & Bish, 1989; Zevin & Kimmel, 1995), some of the more commonly used approaches will be described here along with examples of their use in practical applications.

3.9.2. Phase analysis

There are a number of traditional methods for the estimation of phase abundance in multiphase materials (Zevin & Kimmel, 1995). In summary, these can be divided into two groups:

[1] It is worth noting that the grain-size effect becomes even more of an issue as the divergence of the instrument is decreased with, for example, high-resolution laboratory or synchrotron-based instruments, since fewer crystallites are likely to meet the diffraction condition.

(1) *Indirect methods* – these are usually based on the measurement of total chemical composition, which is then apportioned according to an assumed composition for each phase. A very widely used form of this normative calculation approach is the Bogue method (Bogue, 1929) for the quantitative estimation of Portland cement phases. The limitations in this approach arise when the actual compositions of individual phases vary from those assumed in the calculation. This frequently occurs in the cement industry, where variance in local materials and production conditions can affect detailed phase compositions. Normative calculation has the potential to be unstable when a number of phases in the mixture have similar chemical composition and it cannot be used at all for the limiting case of polymorphs that have identical chemical composition.

(2) *Direct methods* – these are based on a property that is specific to phases of interest in the sample. These methods are often not generally applicable to the entire sample, but are useful in estimating abundances of selected components. Examples include:

   (*a*) Magnetic susceptibility – this is applicable to samples in which component phases have different magnetic properties. The magnetic component can be separated and weighed to determine its weight fraction in the starting material. This approach assumes that the magnetic phase is well separated from non-magnetic phases and accuracy will be reduced when there is a fine inseparable intergrowth of magnetic and non-magnetic components.

   (*b*) Selective dissolution – where the rate and extent of dissolution can be phase dependent, and the weight fraction of the residue is used to determine the fractions of soluble and insoluble components.

   (*c*) Density – involves the physical separation of phases with different densities. As with magnetic separation, this approach assumes that the phase of interest is well separated from other phases.

   (*d*) Image analysis – optical microscopy using thin sections is still frequently used for the analysis of mineralogical samples. Thin sections can be time consuming to prepare and analyse, and the observations can be highly subjective depending on the analyst's experience. While automated image analysis of optical and electron-beam images brings more consistency to the estimation of phase abundance, issues in stereology may still affect the determined phase abundances.

   (*e*) Thermal analysis – where the magnitude of endo- and exothermic features during phase transitions are proportional to the amount of the phases present. This can be effective for well known and characterized phases, but is less useful for new phases or complex multiphase samples where there may be significant overlap in the features in the observed patterns. There may also be difficulty in distinguishing features related to individual minerals, for example H_2O evolution from co-existing hydrated minerals.

   (*f*) Infrared (IR) techniques – these are gaining in popularity, especially in mineral exploration environments because of their portability, speed and ability to measure directly from a cleaned drill core or section. However, because the IR beam only penetrates 1–2 μm into the sample, it is a surface-analysis technique providing a semi-quantitative analysis at best. To work effectively, the method needs to be calibrated using other techniques such as diffraction-based phase analysis.

   (*g*) Powder diffraction may be included in the direct-methods category, as it distinguishes and quantifies phases on the basis of their unique crystal structures, giving the technique broad applicability for crystalline materials.

Quantification from powder diffraction data is reliant on determination of the contribution to the final pattern of each component phase in a mixture. Commonly used methods can be divided into two distinct groups:

(1) The traditional 'single-peak' methods, which rely on the measurement of the intensity of a peak, or group of peaks, for each phase of interest and assumes that the intensity of these peaks is representative of the abundance of the individual phases. This is often not the case because of peak overlap and phase-dependent factors, such as preferred orientation and microabsorption, which affect the relative observed intensities.

(2) Whole-pattern methods, which rely on the comparison of observed diffraction data over a wide range of 2θ with a calculated pattern formed from the summation of individual phase components which have either been (i) measured from pure phase samples, or (ii) calculated from crystal-structure information.

3.9.3. QPA methodology

The integrated intensity $I_{(hkl)\alpha}$ of reflection *hkl* for phase α in a multiphase mixture, measured on a flat-plate sample of infinite thickness using a diffractometer with Bragg–Brentano geometry, is given by (Snyder & Bish, 1989; Zevin & Kimmel, 1995; Madsen *et al.*, 2013)

$$I_{(hkl)\alpha} = \left[\frac{I_0\lambda^3}{32\pi r}\frac{e^4}{m_e^2c^4}\right] \times \left[\frac{M_{hkl}}{2V_\alpha^2}\left|F_{(hkl)\alpha}\right|^2\left(\frac{1+\cos^2 2\theta\cos^2 2\theta_m}{\sin^2\theta\cos\theta}\right)\exp\left(-2B(\sin\theta/\lambda)^2\right)\right] \times \left[\frac{W_\alpha}{\rho_\alpha\mu_m^*}\right], \quad (3.9.1)$$

where I_0 is the incident-beam intensity, λ is the wavelength, e is the charge on an electron, m_e is the mass of an electron, r is the distance from the scattering electron to the detector and c is the speed of light. M_{hkl} and F_{hkl} are the multiplicity and structure factor of the *hkl* reflection, respectively, V_α is the unit-cell volume of phase α, and θ and θ_m are the diffraction angles for the *hkl* reflection and the monochromator (if present), respectively. B is the mean atomic displacement parameter (ADP). W_α and ρ_α are the weight fraction and density of phase α respectively, while μ_m^* is the mass absorption coefficient of the entire sample.

3.9.3.1. *Absorption–diffraction method*

The various terms in equation (3.9.1) are related to the (i) instrument configuration (first set of square brackets), (ii) crystal-structure-related parameters for reflection *hkl* of phase α (second set of square brackets), and (iii) phase-specific and whole-sample parameters including the weight fraction W_α for phase α (last set of square brackets).

The instrument-related and phase-dependent parameters, including phase density, can be grouped together and defined as a constant $C_{i\alpha}$ for the ith reflection of phase α for a specific set of

measurement conditions. This greatly simplifies the relationship between reflection intensity and weight fraction to

$$I_{i\alpha} = C_{i\alpha}\frac{W_\alpha}{\mu_m^*}. \quad (3.9.2)$$

On rearrangement, the weight fraction can be derived from

$$W_\alpha = \frac{I_{i\alpha}\mu_m^*}{C_{i\alpha}}. \quad (3.9.3)$$

Application of equation (3.9.3) (Klug & Alexander, 1974), referred to as the absorption–diffraction method, requires:

(1) the determination of $C_{i\alpha}$ using a rearranged equation (3.9.3) by (i) the preparation of standards with known additions W of phase α_α, (ii) measurement of peak intensity $I_{i\alpha}$ for the standards, and (iii) estimation of the standard sample mass absorption coefficient μ_m^*;
(2) measurement of $I_{i\alpha}$ and estimation of μ_m^* for the unknown samples; and
(3) calculation of W_α *via* equation (3.9.3).

The value of μ_m^* can be estimated by direct measurement of the beam intensity through a sample of known thickness t in a beam of the same wavelength as that used in the XRD data collection. Following measurement of the beam intensity with the sample in (I) and removed from (I_0) the beam, μ_m^* can be calculated using

$$\frac{I}{I_0} = \exp(-\mu_m^*\rho_m t). \quad (3.9.4)$$

However, this usually involves (i) the preparation of an additional, thinner, sample for presentation to the X-ray beam, (ii) in some cases, the addition of a diluent with a low mass absorption coefficient to produce I/I_0 ratios in a range where reasonable accuracy can be achieved, and (iii) knowledge of the 'mass thickness' $\rho_m t$. It should also be noted that there are few commercially available instruments that would be suitable for such measurements due to safety-related issues in accessing the X-ray beam path.

An alternative approach is to calculate μ_m^* from the sum of the products of the theoretical mass absorption coefficient (μ_j^*) of each element (or phase) and the weight fractions (W_j) of all n elements (or phases) in the sample. The elemental composition may be determined, for example, by X-ray fluorescence (XRF) measurement and its use is more accurate than the use of phase composition as it takes into account any amorphous material not represented by peaks in the diffraction pattern but which still contributes to μ_m^*,

$$\mu_m^* = \sum_{j=1}^{n}\mu_j^* W_j. \quad (3.9.5)$$

3.9.3.2. *Internal standard method*

A more general, and experimentally simpler, approach is to eliminate μ_m^* from the analysis altogether *via* the inclusion of an internal standard s in known weight fraction W_s. Substitution of the measured intensity of the jth peak (or group of peaks) of the standard phase, I_{js}, into equation (3.9.2) yields

$$I_{js} = C_{js}\frac{W_s}{\mu_m^*}. \quad (3.9.6)$$

The ratio of equations (3.9.2) and (3.9.6) gives

$$\frac{I_{i\alpha}}{I_{js}} = \frac{C_{i\alpha}}{C_{js}}\frac{W_\alpha}{W_s}. \quad (3.9.7)$$

Since μ_m^* now appears both in the numerator and denominator, its effect on the analysis, and hence the need to measure or calculate it, is removed from the calculation. Rearrangement of equation (3.9.7) yields

$$\frac{I_{i\alpha}}{I_{js}}\frac{W_s}{W_\alpha} = \frac{C_{i\alpha}}{C_{js}} = C_{js}^{i\alpha}, \quad (3.9.8)$$

where $C_{js}^{i\alpha}$ is a calibration constant specific to the phase and internal standard used. Once $C_{js}^{i\alpha}$ has been determined, the weight fraction of the unknown, W_α, can then be determined from

$$W_\alpha = \frac{W_s}{C_{\alpha s}^{ij}}\frac{I_{i\alpha}}{I_{js}}. \quad (3.9.9)$$

This approach, referred to as the *internal standard method*, relies on the determination of $C_{\alpha s}^{ij}$ using known mixtures of standard and analyte phases. The value of $C_{\alpha s}^{ij}$ will be specific to the diffraction peaks used in its determination; if other lines are used in subsequent analysis, then an appropriate value of C will have to be redetermined.

It should be noted that the presence of systematic errors (such as preferred orientation and microabsorption) that influence the measurement of intensity and vary as a function of W_α will not be detected through application of equation (3.9.9). The use of consistent sample-preparation and presentation techniques is required to minimize the effect of these aberrations on the analysis (Zevin & Kimmel, 1995).

3.9.3.2.1. *Selection of an internal standard*

The selection of an appropriate material for use as an internal standard for QPA is not always straightforward. Ideally, the material selected should:

(1) Have a simple diffraction pattern resulting in minimal overlap with peaks of interest in the sample.
(2) Have a mass absorption coefficient similar to that of the sample to avoid introducing microabsorption effects and thus reducing accuracy.
(3) Have minimal sample-related aberrations that may affect observed intensities. For example, it should be fine-grained to ensure minimal grain-size effects on the observed intensities and not be subject to preferred orientation. Importantly, it should have 100% (or known) crystallinity.
(4) Be stable over an extended time and be unreactive, especially for *in situ* studies where it may be subjected to extreme conditions.

Some possibilities for use as internal standard include α-Al_2O_3 (corundum), TiO_2 (rutile), ZnO (zincite), Cr_2O_3 (eskolaite), α-Fe_2O_3 (haematite), CeO_2 (cerianite), CaF_2 (fluorite) and C (diamond). Cline *et al.* (2011) have described the certification of the standard reference material SRM 676a with accurately known amorphous content for use as an internal standard for QPA (see Chapter 3.1). Alternatively, it is possible to use an independent measure (*e.g.* chemical analysis) to derive the concentration of a phase already present in the sample and then to designate it as the internal standard.

Selection of the amount of internal standard to add is often based on folklore or local practices with reported additions ranging from 5 to 50 wt%. Westphal *et al.* (2009) have described the mathematical basis for selecting the optimal internal standard addition in the context of amorphous phase determination. The

amount of internal standard added has a strong influence on the precision of the determination of amorphous content and 'a poor choice can make determination impossible, while a clever choice can enhance the precision'.

With the exception of diamond, all of the phases listed above tend to have absorption coefficients that are too high for use with organic materials. The development and verification of a suitable low-absorption-coefficient standard material that meets the criteria given above remains an important area of research.

3.9.3.3. *Reference intensity ratio methods*

The reference intensity ratio (RIR) (Hubbard *et al.*, 1976; Hubbard & Snyder, 1988) is an instrument-independent phase constant developed specifically for use in quantitative phase analysis and is defined as the ratio of strongest peak of phase α to the strongest peak of standard s. The RIR can be derived directly from equation (3.9.8):

$$\mathrm{RIR}_{\alpha s} = C_{js}^{i\alpha} = \frac{I_{i\alpha}}{I_{js}}\frac{W_s}{W_\alpha}. \tag{3.9.10}$$

In some cases, the strongest lines of either the standard or phase of interest may not be accessible for measurement if, for example, they strongly overlap with peaks from another phase or if they are out of the 2θ range considered. Equation (3.9.10) can be generalized (Hubbard & Snyder, 1988) to use less intense peaks while keeping the same value of RIR:

$$\frac{I_{i\alpha}}{I_{js}}\frac{I_{js}^{\mathrm{rel}}}{I_{i\alpha}^{\mathrm{rel}}}\frac{W_s}{W_\alpha} = \mathrm{RIR}_{\alpha s}, \tag{3.9.11}$$

where I^{rel} is the ratio of the intensity of the peak used for analysis to the most intense peak for the phase. $\mathrm{RIR}_{\alpha,s}$ is now the generalized reference intensity ratio for phase α with respect to standard s.

Quantification of the unknown phase in the presence of a known standard addition can be achieved by the rearrangement of equation (3.9.11):

$$W_\alpha = \frac{I_{i\alpha}}{I_{js}}\frac{I_{js}^{\mathrm{rel}}}{I_{i\alpha}^{\mathrm{rel}}}\frac{W_s}{\mathrm{RIR}_{\alpha s}}. \tag{3.9.12}$$

The generally accepted reference material for QPA *via* the RIR method is corundum because of its relatively simple diffraction pattern, stability and availability as a highly crystalline and pure single phase. If corundum is used, the RIR equates to I/I_c (or 'I over I corundum') for the phase; these are the most commonly reported values in the literature.

RIRs can be determined either by (i) calculation using published crystal-structure information with Rietveld analysis software set to pattern-calculation mode, or (ii) direct measurement by taking the ratio of the strongest peak of the pattern to the intensity of the strongest peak of corundum in a 50/50 weight mixture [or through use of equation (3.9.11) for non-equal proportions]. However, for some phases, there can be ambiguity about which peak is the most intense. For example, the 104 (2.551 Å) and 113 (2.085 Å) peaks of corundum have very similar observed intensities, as do the 111 (3.154 Å) and 022 (1.932 Å) peaks of fluorite. This may lead the analyst to select a peak different from that chosen for reported RIR values.

Collated lists of RIR values for frequently encountered phases can be found in the ICDD database (Fawcett *et al.*, 2017) and Smith *et al.* (1987). It is important to note, however, that the user must be very careful when selecting an appropriate RIR value for their particular experiment. The values of RIR will depend upon the data-collection and measurement strategy employed (for example, peak height, integrated peak area, whole pattern, X-ray wavelength employed and so on) in their derivation. This must match the conditions used in the experiment to which the value is to be applied. In general, RIR values should be determined for the material currently being studied using the methodologies employed rather than relying on published values. Greater accuracy will be achieved if the relative intensities are determined as part of the calibration process using pure samples of the phase and standard or, preferably, samples in which the phases of interest have high and known concentration. If published values of RIR are used, then the determined phase abundances must be referred to as being only semi-quantitative.

3.9.3.4. *Matrix-flushing method*

An important feature of RIR-based techniques is that, once the RIRs are determined for the analyte phases of interest, the standard phase does not need to be present in the sample. The effect of the sample mass absorption coefficient is also removed by taking the ratio of the intensity of phase α to another unknown phase β. Hence the ratio of the weight fractions of the two phases can be derived from

$$\frac{W_\alpha}{W_\beta} = \frac{I_{i\alpha}}{I_{j\beta}}\frac{I_{j\beta}^{\mathrm{rel}}}{I_{i\alpha}^{\mathrm{rel}}}\frac{\mathrm{RIR}_{\beta s}}{\mathrm{RIR}_{\alpha s}}. \tag{3.9.13}$$

For a system comprising n phases, equation (3.9.13) allows the derivation of $n-1$ weight fraction ratios. Chung (1974*a*,*b*) has demonstrated that, if all components are crystalline and included in the analysis, an additional constraint of the following form can be included:

$$\sum_{k=1}^{n} W_k = 1.0. \tag{3.9.14}$$

This forms a system of n linear equations which can be solved to give the weight fractions of all components in the analysis according to (Chung, 1974*a*,*b*; Snyder & Bish, 1989)

$$W_\alpha = \frac{I_\alpha}{\mathrm{RIR}_{\alpha s} I_\alpha^{\mathrm{rel}}}\left(\sum_{k=1}^{n}\frac{I_k}{\mathrm{RIR}_{ks} I_k^{\mathrm{rel}}}\right)^{-1}. \tag{3.9.15}$$

The weight fractions analysed *via* this method are correct relative to each other but may not be correct in an absolute sense if unidentified or amorphous materials are present in the sample. In this case, the reported phase abundances will be overestimated. The addition of an internal standard to the system, or knowledge of the amount of a component phase determined by another technique, allows calculation of the absolute amount $W_{\alpha(\mathrm{abs})}$ of each phase [equation (3.9.16)] and thus the derivation of the amount W_{unk} of unknown (amorphous and/or unidentified) components [equation (3.9.17)].

$$W_{\alpha(\mathrm{abs})} = W_\alpha \times \frac{W_{\mathrm{std(known)}}}{W_{\mathrm{std(meas)}}}, \tag{3.9.16}$$

$$W_{\mathrm{unk}} = 1.0 - \sum_{k=1}^{n} W_{k(\mathrm{abs})}, \tag{3.9.17}$$

where $W_{\alpha(\mathrm{abs})}$ is the absolute weight fraction of phase α, $W_{\mathrm{std(known)}}$ is the known weight fraction of the standard added to the sample, $W_{\mathrm{std(meas)}}$ is the weight fraction of the standard

reported by equation (3.9.15) and W_{unk} is the weight fraction of the unidentified and/or amorphous component in the mixture.

If an internal standard has been used, then initial calculation of its concentration *via* equation (3.9.15) may be:

(i) the same as the weighed amount, indicating that there are unlikely to be amorphous or unidentified phases present;
(ii) greater than the weighed amount, indicating that amorphous or unidentified phases may be present; or
(iii) less than the weighed amount, indicating operator error or the use of invalid RIR or I^{rel} values.

3.9.3.5. *Full-pattern fitting methods*

The quantitative XRD techniques described above have traditionally been applied using phase intensity estimates derived from either single peaks or a small group of peaks. This approach can be effective when there is minimal peak overlap but becomes less useful in complex phase systems where it may be difficult to identify freestanding peaks in the pattern. In addition, the presence of sample-related effects such as preferred orientation skew the measured intensities from what would be expected from an ideal powder diffraction pattern, thus reducing the expected accuracy.

Some of these effects can be partially overcome by using full-pattern fitting methods (Smith *et al.*, 1987; Batchelder & Cressey, 1998; Chipera & Bish, 2002, 2013; Eberl, 2003; Toraya & Tsusaka, 1995; Cressey & Schofield, 1996), where wide-range diffraction patterns of phases of interest are scaled, summed and compared with the observed diffraction data in a least-squares minimization process. The method relies on the generation of a library of standard patterns for each phase expected in the analysis collected under the same instrumental conditions as those used in subsequent analyses. The selection of standards that are a good match for the phases in the unknown sample is a critically important step. While the library will normally contain patterns of well ordered phases, it can also include patterns for less well ordered material such as glasses, polymers, clay minerals and gels, thus allowing their direct quantification. Where it is not possible to obtain a measured pattern, calculated patterns may also be included in the library.

Weight fractions are obtained by the solution of simultaneous equations that take into account the scale factors of the individual components and the mass absorption coefficients derived from knowledge of the elemental composition of each phase.

Alternatively, the contribution of library patterns to observed data can be normalized by scaling phases to an internal standard, typically corundum, using an RIR approach. Given the compositional and structural variability of some phases, especially in mineralogical applications, RIRs measured using the same minerals as those to be analysed are preferred to reported RIRs. Toraya (Toraya 2016*a*,*b*) has devised a QPA method which uses observed integrated peaks intensities measured of a wide 2θ range. Phase calibration constants are calculated using only their chemical formula weight and the sum of the square of the number of electrons in the formula unit. While the method is effective for wide-range data, it cannot be applied to single-peak data or data that cover only a limited 2θ range.

The full-pattern fitting method is relatively easy to use and can be applied to difficult samples containing highly disordered materials. For some disordered phases where no crystal structure is available and where peak overlap means that individual peak intensities cannot be measured, full-pattern fitting may be the most appropriate approach to QPA. The major limitations of the method include the need (i) to define and subtract the pattern background, with a subsequent impact on QPA, and (ii) to obtain or generate a library of standard patterns of the phases of interest. The use of an internal standard is recommended and the method is best applied when all standard patterns have first been normalized to an internal standard intensity (Chipera & Bish, 2002, 2013).

3.9.3.6. *Rietveld-based QPA*

The advent of the Rietveld method (Rietveld, 1969) and its extension into the field of QPA (Bish & Howard, 1988; Hill, 1983; Hill & Howard, 1987; O'Connor & Raven, 1988; Taylor, 1991) has brought some significant benefits when compared with the conventional single-peak and pattern-addition methods. Recent surveys (Madsen *et al.*, 2001; Scarlett *et al.*, 2002) show that the majority of participants, greater than 75%, use a Rietveld-based approach for QPA. The benefits derive from (Hill, 1991; Kaduk, 2000):

(i) The use of the entire diffraction pattern. Depending on the 2θ range of the data and the crystallography of the component phases, this may involve hundreds or thousands of reflections rather than the few peaks in conventional methods. This helps to minimize the impact of some systematic sample-related effects such as preferred orientation and extinction.
(ii) The ability to accurately deconvolute overlapping peaks to extract the component intensities, thus allowing more complex patterns to be analysed. The development of fundamental-parameters models (Bergmann *et al.*, 1998, 2000; Cheary & Coelho, 1992; Cheary *et al.*, 2004), which aim to distinguish instrument from sample contributions to the diffraction pattern, minimizes the number of profile parameters that need to be refined, further enhancing this profile-fitting step.
(iii) Refinement of the crystal structure, when supported by the data, to minimize differences between the intensities in the calculated and observed patterns. This brings additional information such as systematic changes in structure parameters from published data.
(iv) The ability to model some remaining systematic effects such as preferred orientation or anisotropic crystallite size/strain peak broadening.

The Rietveld method uses a least-squares procedure to minimize the difference between a calculated pattern and the measured data. The calculated pattern is derived from a model containing crystal-structure information for each phase included in the analysis, convoluted with expressions describing peak shape and width, along with functions to correct systematic variances such as preferred orientation. The calculated pattern is multiplied by an overall scaling factor which may be equated to the peak intensities ($I_{i\alpha}$) considered by the single-peak methods. The Rietveld scale factor for phase α, S_α, can be defined as (Bish & Howard, 1988; Hill, 1991; Hill & Howard, 1987; O'Connor & Raven, 1988)

$$S_\alpha = \left[\frac{K}{V_\alpha^2}\right]\left[\frac{W_\alpha}{\rho_\alpha}\right]\frac{1}{2\mu_m^*}, \tag{3.9.18}$$

where K is an 'experiment constant' used to put W_α on an absolute basis, and V_α, W_α and ρ_α are the volume of the unit cell, the weight fraction and the density for phase α, respectively.

Since equation (3.9.18) inherently contains the weight-fraction information, it can be rearranged to derive W_α:

$$W_\alpha = \frac{S_\alpha \rho_\alpha V_\alpha^2 \mu_m^*}{K}. \quad (3.9.19)$$

O'Connor & Raven (1988) and Bish & Howard (1988) have shown that K is dependent only on the instrumental conditions and is independent of individual phase and overall sample-related parameters. Therefore a single measurement is sufficient to determine K for a given instrument configuration and set of data-collection conditions. Determination of K may be carried out by (i) a measurement of either a pure phase, or a phase of known proportion in a mixture, separately from the measurement of the actual unknown mixture, or (ii) using a phase that is present in the sample in a known amount. The value of K calculated in this way will be appropriate for the calibration of subsequent measurements as long as all instrumental and data-collection conditions remain the same as those used in its determination.

For each phase, the density ρ_α can be calculated from the published (or refined) crystal-structure information using

$$\rho_\alpha = \frac{ZM_\alpha}{V_\alpha}, \quad (3.9.20)$$

where ZM is the mass of the unit-cell contents (Z is the number of formula units in the unit cell and M is the molecular mass of the formula unit) and V is the unit-cell volume.[2]

Substitution of equation (3.9.20) in equation (3.9.19) shows that

$$W_\alpha = \frac{S_\alpha (ZMV)_\alpha \mu_m^*}{K}. \quad (3.9.21)$$

In this context, $(ZMV)_\alpha$ is the 'phase constant' and can be calculated from published or refined crystal-structure information alone. It is worth noting that, if the crystal structure is refined as part of the analysis, ZMV is updated and hence becomes a dynamic phase constant.

The methodology embodied in equation (3.9.21) is important in many applications in that it produces, within the limits of experimental error, *absolute phase abundances* and is referred to hereafter as the *external standard* approach. While the use of a phase that already exists within the sample to determine K may be considered as an internal standard approach, in some applications, including *in situ* studies, that phase may be removed from the system through, for example, decomposition or dissolution. However, the value of K remains valid for subsequent determination of phase abundances provided that the instrumental and data-collection conditions do not change.

Equation (3.9.21) is directly applicable to the analysis of those phases for which detailed crystal-structure information is available. For phases where only a partial structure (for example, an indexed unit cell but no atom coordinates or site-occupation factors) is available, an empirical ZMV can be derived using mixtures of the phase of interest with known amounts of a well characterized standard (Scarlett & Madsen, 2006). QPA of phases with partial structure is also possible through the use of equation (3.9.19), but an estimate of the phase density, obtained through direct measurement, is required.

The limitations of the approach embodied in equations (3.9.19) and (3.9.21) derive from the need to (i) conduct a measurement of K and (ii) estimate the value of the mass absorption coefficient μ_m^* for the sample(s) used to determine K, as well as for each sample of interest. However, similar to the earlier discussion about the single-peak methods, μ_m^* can be determined by direct measurement or calculation using equations (3.9.4) or (3.9.5), respectively. The benefits that can be derived from the extraction of the absolute, rather than relative, phase abundances, make it worth pursuing in many analytical situations. For example, in time-resolved studies where phases transform and material is lost in the course of reaction, the calculation of relative abundances summed to 100% may give a misleading impression of increased amounts of the remaining phases.

In some diffraction instruments, there may be decay in the incident-beam intensity during the course of measurement. This may happen on the timescale of months for a laboratory-based instrument owing to X-ray tube ageing, or on the scale of minutes at a synchrotron instrument where the storage-ring current is only refreshed once or twice per day. In this case, the change in incident intensity can be taken into account by incorporating an additional term into equation (3.9.21):

$$W_{\alpha i} = \frac{S_{\alpha i} (ZMV)_\alpha \mu_m^*}{K} \frac{I_0}{I_i}, \quad (3.9.22)$$

where I_0 and I_i are the incident beam intensities present during the determination of K and the collection of data set i, respectively.

The need to measure K, and measure or calculate μ_m^*, serves to increase the overall experimental difficulty and can be eliminated in ways analogous to those used in the single-peak methodology described earlier. For a simple two-phase mixture where both phases, α and β, are 100% crystalline, the sum of their weight fractions W_α and W_β equals unity and can be expressed as (Bish & Howard, 1988)

$$W_\alpha = \frac{W_\alpha}{W_\alpha + W_\beta}. \quad (3.9.23)$$

Substitution of equation (3.9.21) for phases α and β in equation (3.9.23) results in

$$W_\alpha = \frac{S_\alpha (ZMV)_\alpha}{S_\alpha (ZMV)_\alpha + S_\beta (ZMV)_\beta}. \quad (3.9.24)$$

Alternatively, in a multiphase sample, the addition of an internal standard s in known amount W_s and taking the ratio of equation (3.9.21) for analyte and standard phases provides the relationship

$$W_\alpha = W_s \frac{S_\alpha (ZMV)_\alpha}{S_s (ZMV)_s}. \quad (3.9.25)$$

The method embodied in equation (3.9.25) is analogous to the *internal standard* approach in equation (3.9.9) and also serves to produce *absolute phase abundances* $W_{\alpha(\mathrm{abs})}$. Once again, the benefit accruing from the use of absolute phase abundances is the ability to estimate the presence and amount of any amorphous and/or unidentified phases $W_{(\mathrm{unk})}$ through application of equations (3.9.16) and (3.9.17).

Hill & Howard (1987) and Bish & Howard (1988) have adapted the matrix-flushing method of Chung (1974*a*,*b*) to the Rietveld analysis context. By constraining the sum of the analysed weight fractions to the assumed concentration of the crystalline components (usually unity), the weight fraction of phase α in an n-phase mixture is given by the relationship[3]

[2] When calculating phase density from crystallographic parameters, a factor of $1.6604 = 10^{24}/6.022 \times 10^{23}$ is needed to convert ρ in a.m.u. Å^{-3} to g cm^{-3}.

[3] It should be noted that the implementation of the matrix-flushing method by Bish and Howard retains the use of phase density, but their approach is essentially the same as that of Hill and Howard.

$$W_\alpha = \frac{S_\alpha (ZMV)_\alpha}{\sum_{k=1}^{n} S_k (ZMV)_k}. \qquad (3.9.26)$$

The use of equation (3.9.26) in QPA again eliminates the need to measure the instrument calibration constant and estimate the sample mass absorption coefficient. However, the necessity of normalizing the sum of the analysed weight fractions to unity only produces the correct *relative phase abundances*. This approach is the most widely used in Rietveld-based QPA and is almost universally coded into Rietveld analysis programs. If the sample contains amorphous phases and/or minor amounts of unidentified crystalline phases, the analysed weight fractions will be overestimated. Where absolute phase abundances are required in, for example, the derivation of reaction mechanisms in *in situ* studies, then one of the methods that produces absolute phase abundances must be used.

3.9.4. Demonstration of methods

The sample 1 suite from the IUCr Commission on Powder Diffraction (CPD) round robin on QPA (Madsen *et al.*, 2001) provides a useful basis for demonstrating the applicability some of the methods described above. Sample 1 was designed to provide a relatively simple analytical system in order to determine the levels of accuracy and precision that could be expected under ideal conditions. The key design criteria required that the phases exhibit little peak overlap in the low-angle region of the diffraction pattern and the samples have at least one freestanding peak for each phase in the *d*-spacing range 3.7 to 1.9 Å.

The three components (corundum, α-Al_2O_3; fluorite, CaF_2; and zincite, ZnO) were prepared in a ternary design to provide a total of eight different mixtures in order to cover as wide a range of composition as possible for each phase. The result is that each phase is present in the suite with concentrations of approximately 1, 4, 15, 33, 55 and 95 wt%. The exact compositions (Madsen *et al.*, 2001) can be found in Table 3.9.1. The unique chemical composition of the component phases also allowed the weighed compositions to be confirmed by measurement of total elemental composition using X-ray fluorescence (XRF) methods.

Data sets were collected from three replicates of the eight mixtures using a Philips X'Pert diffractometer equipped with a Cu long fine focus tube operated at 40 kV and 40 mA. The beam path was defined with 1° divergence, 0.3 mm receiving and 1° scatter slits. A curved graphite post-diffraction monochromator was fitted to eliminate $K\beta$ radiation. Data were collected from 15 to 145° 2θ in increments of 0.02° using a counting time of 1.5 s per step. These data sets are available as supporting information from http://it.iucr.org/ for any reader wishing to develop and test their skills in various methods.

For the single-peak methods, the net intensity for all peaks in the range 22 to 65° 2θ was extracted using a fundamental-parameters approach to peak fitting coded in the *TOPAS* software package (Bruker AXS, 2013). The choice of peak profile type is important, since any misfit will be reflected in the estimation of peak area and hence in the QPA. Unless otherwise stated, QPA was undertaken using the strongest peak in the pattern for each phase (corundum 113, d = 2.085 Å; fluorite 022, d = 1.932 Å; zincite 011, d = 2.476 Å). The average values for these peaks can be found in Table 3.9.2. For those methods requiring knowledge of the mass absorption coefficient, μ_m^* for each sample was calculated from the XRF chemical analysis results.

Table 3.9.1
Weighed composition (weight fraction) of the eight mixtures comprising sample 1 in the IUCr CPD round robin on QPA (Madsen *et al.*, 2001)

Sample	Corundum	Fluorite	Zincite
1A	0.0115	0.9481	0.0404
1B	0.9431	0.0433	0.0136
1C	0.0504	0.0136	0.9359
1D	0.1353	0.5358	0.3289
1E	0.5512	0.2962	0.1525
1F	0.2706	0.1772	0.5522
1G	0.3137	0.3442	0.3421
1H	0.3512	0.3469	0.3019

Table 3.9.2
Average values (n = 3) of net peak intensity derived using profile fitting for the strongest peaks of corundum (113), fluorite (022) and zincite (011)

The figures in parentheses are the standard deviations of the means. The sample mass absorption coefficient μ_m^* was calculated from the XRF-L determined composition.

Sample	Corundum	Fluorite	Zincite	μ_m^* (cm^2 g^{-1})
1A	34.8 (0.6)	8958.7 (33.0)	509.9 (6.0)	93.02
1B	6561.3 (28.6)	1095.5 (7.1)	474.3 (3.8)	34.45
1C	244.4 (0.9)	250.9 (10.1)	22898.0 (37.0)	49.03
1D	474.5 (3.5)	6559.6 (2.8)	5468.5 (9.5)	71.71
1E	2525.3 (27.9)	4835.5 (27.0)	3370.7 (16.3)	53.17
1F	1251.3 (7.8)	2935.8 (9.0)	12494.9 (22.4)	52.67
1G	1295.0 (8.7)	5041.7 (17.0)	6787.9 (26.6)	59.64
1H	1436.5 (7.3)	5132.0 (13.6)	5996.8 (59.5)	59.10

3.9.4.1. *Absorption–diffraction method*

In this method, the QPA of each phase is conducted independently of the others. For each phase, the determination of a specific calibration constant, C, was achieved using a rearranged equation (3.9.3). The sample where the relevant phase was present at about 55 wt% (sample 1E for corundum, 1D for fluorite and 1F for zincite) was taken to be the calibration sample.

For fluorite the determination of C proceeded using

$$C_{i,\alpha} = I_{i,\alpha} \frac{\mu_m^*}{W_\alpha} = 6559.6 \times \frac{71.71}{0.5358} = 877\,919. \qquad (3.9.27)$$

All data sets were then analysed using equation (3.9.3), as demonstrated here using sample 1H.

$$W_\alpha = I_{i,\alpha} \frac{\mu_m^*}{C_{i,\alpha}} = 5132.0 \times \frac{59.1}{877919} = 0.3455, \qquad (3.9.28)$$

compared with a value of 0.3469 added to the sample by weight. Fig. 3.9.1 shows the analysed concentration for all 24 fluorite measurements along with the bias from the known values. The bias (analysed − known) all fall within the range −0.3 to 0.5 wt% with no systematic bias as a function of concentration. The similar results achieved for corundum and zincite demonstrate the validity of the approach where there is minimal peak overlap.

3.9.4.2. *Internal standard method*

Application of the internal standard method normally requires the addition of an appropriate phase in known amount to each sample to be analysed. In order to use this data for demonstration of the internal standard method, it is necessary to designate one of the existing phases as the internal standard. Sample 1H has been used to derive the calibration constant, with fluorite considered to be the phase of interest while zincite is designated

as the internal standard. The intensities (Table 3.9.2) and known concentrations (Table 3.9.1) of these phases can then be used to derive $C_{\alpha s}^{ij}$ from equation (3.9.8) to eliminate the need to know or measure μ_m^* for the sample.

$$\frac{I_{\text{fluorite}}}{I_{\text{zincite}}}\frac{W_{\text{zincite}}}{W_{\text{fluorite}}} = C_{\alpha s}^{ij} = \frac{5132.0}{5996.8} \times \frac{0.3019}{0.3469} = 0.7448. \qquad (3.9.29)$$

Analysis of the unknowns (Fig. 3.9.2) then proceeds *via* equation (3.9.9) and is demonstrated here using sample 1D:

$$W_{\text{fluorite}} = \frac{W_{\text{zincite}}}{C_{\alpha s}^{ij}}\frac{I_{\text{fluorite}}}{I_{\text{zincite}}} = \frac{0.3289}{0.7448}\frac{6559.6}{5468.5} = 0.5297, \qquad (3.9.30)$$

compared with a value of 0.5358 added to the sample by weight.

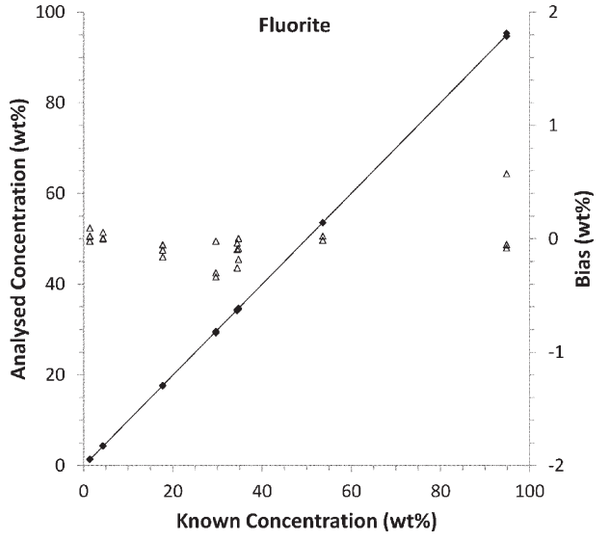

Figure 3.9.1
Plot of the analysed concentration (black diamonds – left axis) and the bias (open triangles – right axis) expressed as wt% for fluorite using the absorption–diffraction method. The analysis was calibrated using sample 1D, which has a fluorite concentration of 53.58 wt%.

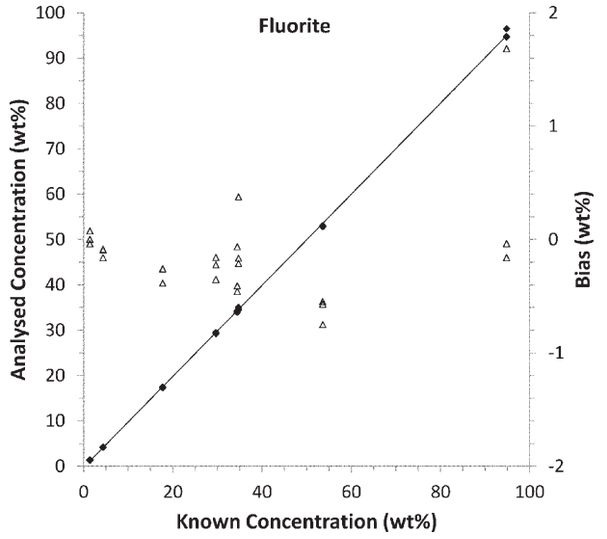

Figure 3.9.2
Plot of the analysed concentration (black diamonds – left axis) and the bias (open triangles – right axis) expressed as wt% for fluorite using the internal standard method with zincite designated as the internal standard. The analysis was calibrated using sample 1H where the fluorite and zincite concentrations are 34.69 and 30.19 wt%, respectively.

3.9.4.3. *Reference intensity ratio*

For this exercise, the peak intensities and phase concentrations in Tables 3.9.1 and 3.9.2 for sample 1H can be used to determine the RIRs for fluorite and zincite.

$$\text{RIR}_{\text{fluorite}} = \frac{5132.0}{1436.5} \times \frac{0.3512}{0.3469} = 3.617, \qquad (3.9.31)$$

$$\text{RIR}_{\text{zincite}} = \frac{5996.8}{1436.5} \times \frac{0.3512}{0.3019} = 4.856. \qquad (3.9.32)$$

These RIRs should be compared with reported values for fluorite in the ICDD database (ICDD, 2015) which have an average of 3.83 (n = 33) but range from 2.40 to 4.21. For zincite the reported RIR values have an average of 5.24 (n = 50) and range from 4.50 to 5.87. The discrepancies in the various reported values of the RIRs highlight the need to determine them under the same conditions as the samples being analysed if the highest accuracy is to be achieved.

Fig. 3.9.3 shows the RIR values calculated from all 24 (eight samples, three replicates each) measurements for fluorite and zincite plotted as a function of corundum concentration. At intermediate concentrations there is quite good agreement between the determined values. However, there are significant deviations at low corundum concentration, resulting in insufficient measured intensity in the corundum peak to ensure sufficient accuracy in the RIR. Hence, care should be taken to ensure that there are sufficient counts in the peaks used to determine the RIR. In addition, a low concentration automatically means that there are fewer grains contributing to the diffraction process; hence particle statistics may also present a significant problem.

The presence of other sample-related aberrations that affect the measured intensities also needs to be considered. For example, microabsorption may affect measured RIR values differently in different concentration ranges. The impact of such effects on the analysis is reduced by their inclusion in the measured RIR provided that variation induced by, for example, sample preparation can be kept to a minimum.

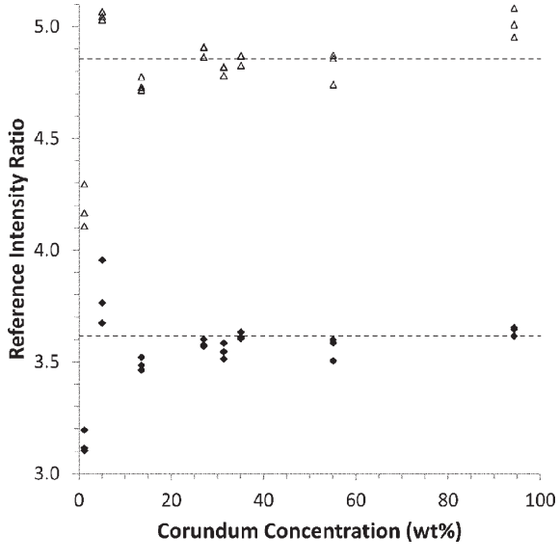

Figure 3.9.3
Plot of the 24 determined RIR values for fluorite (black diamonds) and zincite (open triangles) as a function of corundum concentration. The dashed lines represent the average RIR values for fluorite (lower) and zincite (upper) determined from the three replicates of sample 1H where all phases have approximately equal concentration.

3.9.4.4. *Matrix flushing*

Once the correct value of RIR is determined for each phase, the matrix-flushing method can be applied using equation (3.9.15). For fluorite in sample 1D, the calculation proceeds as follows:

$$W_{\text{fluorite}} = \frac{I_{\text{fluorite}}/\text{RIR}_{\text{fluorite}}}{\sum_{k=1}^{n} I_k/\text{RIR}_{ks}} = \frac{6559.6/3.617}{474.5/1.0 + 6559.6/3.617 + 5468.5/4.856} = 0.5312, \quad (3.9.33)$$

compared with a value of 0.5358 added to the sample by weight. Fig. 3.9.4 shows the bias for fluorite in all samples analysed by the matrix-flushing method. Once again, there is good agreement between the weighed and analysed amounts. However, it is worth reiterating that this method normalizes the sum of all analysed weight fractions to unity. If amorphous or non-analysed phases are present in the sample, then the weight fractions will be overestimated relative to their absolute abundances.

3.9.4.5. *Rietveld-based methods*

The strengths and weaknesses of some of the methods described in Section 3.9.3 are highlighted through a study of the mechanism and kinetics of nucleation and crystal growth in the context of the Bayer process for the extraction of aluminium from bauxite ores (Webster *et al.*, 2010). Specifically, the experiments utilize synthetic Bayer liquors, consisting of Al-loaded caustic solutions to which a variety of seed material is added. Several polymorphs of $Al(OH)_3$ (gibbsite, bayerite and nordstrandite) crystallize from solution onto the seed material. The rate of crystallization and the ratio of the phases formed depend on the sample conditions used, including the Al and caustic concentrations in solution, as well as sample temperature.

The mechanism and rate of crystallization were followed by collecting XRD data at the powder-diffraction beamline of the Australian Synchrotron[4] over a period of about 3 h. The diffractometer incorporates a Mythen detector (Schmitt *et al.*, 2003) which allows for the simultaneous collection of 80° 2θ of the diffraction pattern. A wavelength of 0.826 Å was used to ensure adequate penetration of the beam in the sample. The sample environment (Madsen *et al.*, 2005; Norby *et al.*, 1998) consisted of a 1-mm quartz glass capillary containing a slurry of the seed and Bayer liquor heated to temperatures between 333 and 348 K using a hot-air blower.

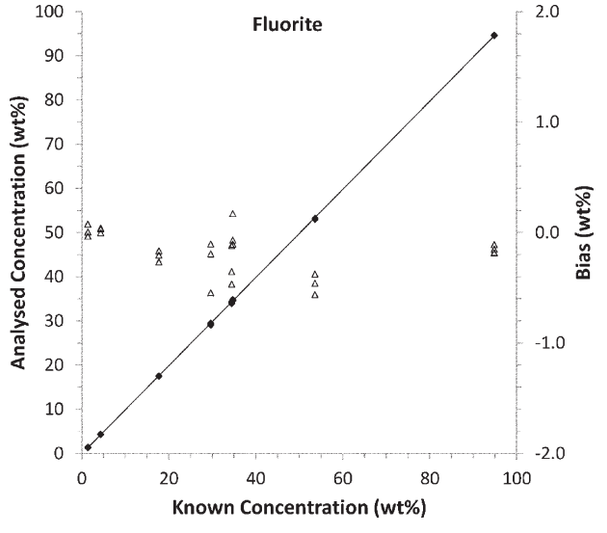

Figure 3.9.4
Plot of the analysed concentration (black diamonds – left axis) and the bias (open triangles – right axis) expressed as wt% for fluorite using the matrix-flushing method with RIRs of 1.0, 3.617 and 4.856 for corundum, fluorite and zincite, respectively. The RIRs were determined using sample 1H where the corundum, fluorite and zincite concentrations are 35.12, 34.69 and 30.19 wt%, respectively.

The data were analysed using *TOPAS* (Bruker AXS, 2013), where a learned-profile approach to peak modelling was used with an empirical instrument width and shape contribution determined using the NIST SRM660 LaB_6 profile standard. For the samples in the study, refined parameters included 2θ zero offset, a Chebychev polynomial pattern background and, for each phase, the Rietveld scale factor, crystallite size and strain, and unit-cell dimensions.

A number of different approaches were used to extract the phase abundances at each stage of the reaction. Initially, QPA was derived using equation (3.9.26); the value that many Rietveld analysis programs output as their first estimate of phase abundance. Fig. 3.9.5 shows the QPA output from an *in situ* experiment in which goethite (FeOOH) was added as the seed.

At the start of the experiment, prior to the crystallization of any of the $Al(OH)_3$ polymorphs, Fig. 3.9.5 shows that the reported concentration of the goethite seed is 100 wt% since it is the only phase represented in the analysis at that time. On formation of gibbsite, bayerite and nordstrandite, the goethite concentration appears to decrease progressively to about 65 wt% while the total $Al(OH)_3$ concentration reaches about 35 wt% at the end of the experiment. However, these figures are in disagreement with (i) the fact that goethite is unlikely to dissolve or otherwise be consumed in this system (Murray *et al.*, 2009), (ii) the known addition of goethite to the sample (14.13 wt%) and (iii) the total amount of $Al(OH)_3$ available from solution (15.92 wt%). The problem with the QPA in this case arises from the fact that only the crystalline components are considered in the analysis and that equation (3.9.26) normalizes the sum of their analysed weight fractions to unity. However, aluminium, which is in solution at the start of the run, forms crystalline phases continuously throughout the reaction after an initial induction period. In order to overcome the anomalies in the QPA results, it is necessary to consider the sample as a whole; that is, the concentration of both the solid and liquid components in the X-ray beam for the duration of the experiment.

In this sample, the concentration of the goethite seed was 14.13 wt% in the slurry injected into the sample capillary. If the assumption is made that, in this environment, goethite is unreactive and its concentration will not change during the reaction, it can be used as an internal standard to put the $Al(OH)_3$ concentrations on an absolute basis. The QPA results derived using the internal standard or 'spiked' approach in equation (3.9.25) are shown in Fig. 3.9.6.

The goethite concentration is fixed at the known addition (14.13 wt%) at the start of the experiment. However, the concentrations of the $Al(OH)_3$ polymorphs are now put on an absolute scale, thus allowing derivation of more meaningful reaction mechanisms.

If, however, there is residual doubt about the reactivity of the goethite, it may be necessary to use the external standard approach embodied in equation (3.9.21). In this case, the value for the instrument constant, K, can be derived using the Rietveld scale factor, ZMV and the known addition of goethite in a

[4] Australian Synchrotron beamtime award number AS091/PD1035.

rearranged equation (3.9.21). For this determination, the goethite scale factor from the first few data sets, prior to the start of the reaction, was averaged to minimize any errors that may be introduced by counting statistics. The value of the sample mass absorption coefficient μ_m^* was set to an arbitrary value of unity for both the determination of K and all subsequent analyses, since the overall chemical content of the capillary, and hence the attenuation of the X-ray beam, does not change during the reaction.

This experimental work was conducted at the Australian Synchrotron where the storage-ring current was boosted every 12 h. Between these times the current, and hence the incident-beam intensity, decays, resulting in what amounts to a change in the 'instrument configuration'. This requires a modification of the K value and subsequent calculation of concentration to compensate for the changing incident intensity using equation (3.9.22).

Fig. 3.9.7 now shows the results of QPA derived from equation (3.9.22). In this case the concentrations of the $Al(OH)_3$ polymorphs are similar to those in Fig. 3.9.6. However, since the phase abundances are derived using an external standard approach, any changes in the apparent goethite concentration can now be monitored. Fig. 3.9.7 shows that the goethite concentration did not change significantly in the early stages of the experiment ($t < 10$ min) before $Al(OH)_3$ crystallization was observed but there is a small, systematic decrease in the apparent goethite concentration as the experiment progresses. At the end of the experiment, the goethite concentration appears to be lower by about 1% relative to the concentration at the start.

This apparent decrease could be due to a number of causes including (i) poor correction for beam-intensity changes or (ii) solid material moving about in the capillary with some movement out of the X-ray beam. Alternatively, the decrease could be attributed to the 'shielding' of the goethite from the X-ray beam by the $Al(OH)_3$ phases as they form and coat the goethite particles. This decrease could then be used to obtain an average thickness of the $Al(OH)_3$ phases on the seed particles. This layer was calculated to be about 5.5 μm (assuming a linear absorption coefficient of 9.5 cm^{-1} for gibbsite at 0.826 Å) resulting in an overall particle size of about 11 μm at the end of the run (the goethite particles are about 0.2 × 2 μm and hence do not contribute significantly to the overall particle size). These values are in good agreement with independent studies (Webster *et al.*, 2010) where the gibbsite was examined using scanning electron microscopy (SEM) techniques (Fig. 3.9.8) following crystallization under similar conditions to those used here.

3.9.5. Alternative methods for determination of calibration constants

3.9.5.1. *Standardless determination of the phase constant C*

In order to determine the phase calibration constant C, it is common to obtain (i) a pure sample of the phase of interest that accurately reflects the form of the phase in the samples to be analysed, or (ii) a multiphase sample in which the phase concentration is known by other means (for example, chemical analysis or point counting). In some systems, there may be insufficient sample available to risk 'contaminating' it with an internal standard, especially if the material needs to be analysed using other techniques. The addition of an internal standard may also introduce microabsorption problems or increase the complexity of patterns that are already highly overlapped. For other situations, the time frame demanded for the analysis may prohibit the time-consuming procedures of standard addition, data collection and separate determination of the phase calibration constant.

Zevin & Kimmel (1995) have described an approach to the derivation of phase constants which relies on having a suite of samples to be analysed that (i) have the same phases present in all samples and (ii) exhibit a wide range of composition of these phases in various samples in order to stabilize the analysis. If we reconsider the relationship between the weight fraction W_α and the observed intensity [equation (3.9.3)],

$$W_\alpha = \frac{I_\alpha \mu_m^*}{C_\alpha}, \tag{3.9.34}$$

and assume that all phases in the system are known and included in the analysis, we can introduce the additional constraint that the sum of all W_α's is unity (or at least a known value):

$$\sum_{j=1}^{n} W_j = 1.0. \tag{3.9.35}$$

In a system of n samples containing m phases, we can explicitly write the relationships expressed in equations (3.9.34) and (3.9.35) as a set of simultaneous equations:

$$\begin{aligned}
1.0 &= \frac{1}{C_1} I_{11}\mu_1^* + \frac{1}{C_2} I_{12}\mu_1^* + \ldots + \frac{1}{C_m} I_{1m}\mu_1^*, \\
1.0 &= \frac{1}{C_1} I_{21}\mu_2^* + \frac{1}{C_2} I_{22}\mu_2^* + \ldots + \frac{1}{C_m} I_{2m}\mu_2^*, \\
1.0 &= \frac{1}{C_1} I_{n1}\mu_n^* + \frac{1}{C_2} I_{n2}\mu_n^* + \ldots + \frac{1}{C_m} I_{nm}\mu_n^*,
\end{aligned} \tag{3.9.36}$$

where μ_n^* is the mass absorption coefficient for the nth sample.

Knudsen (1981) has described a modification to this approach by including an internal standard in each of the samples to be analysed and using the ratio of intensities of the analyte and internal standard phases in place of the I_{nm} in equation (3.9.36). While this eliminates the need to determine and use the mass absorption coefficient, the tedious procedure of adding and mixing an internal standard is required for each sample and for reasons described above may not be appropriate.

The relationships embodied in equations (3.9.36) can be expressed more simply in matrix notation as

$$\mathbf{L}' = \mathbf{I}'\mathbf{C}', \tag{3.9.37}$$

where $\mathbf{L}'$ is a column vector (dimensions $1 \times n$) containing the known (or assumed) sum of weight fractions for each sample (unity in this case), $\mathbf{C}'$ is a column vector (dimensions $1 \times m$) containing the calibration constants for each phase and $\mathbf{I}'$ is a rectangular matrix (dimensions n rows × m columns) containing the measured peak intensities (or scale factors) for each phase multiplied by the sample mass absorption coefficient.

A least-squares solution of equation (3.9.37) to derive the value for C for each phase can be calculated using matrix-manipulation methods (Knudsen, 1981):

$$\mathbf{C}' = \left(\mathbf{I}'^T\mathbf{I}'\right)^{-1}\mathbf{I}'^T\mathbf{L}', \tag{3.9.38}$$

where the superscripts T and -1 represent the transpose and inverse matrix functions, respectively.

Accuracy in the calculation of the individual values of C is improved by having (i) phases of the same or similar composition in all samples and (ii) a wide range of concentrations of each phase across the sample suite. These conditions may be met in,

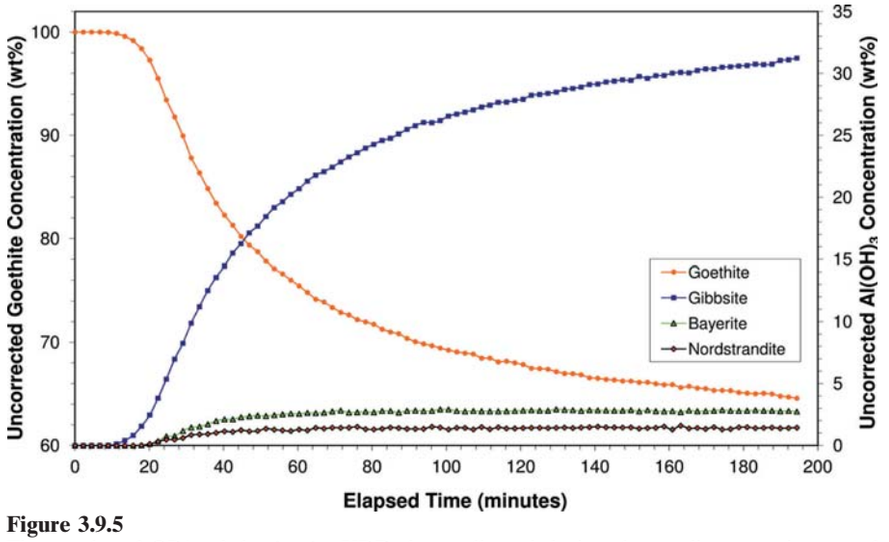

Figure 3.9.5
The results of QPA of the *in situ* XRD data collected during the seeding experiments of Webster *et al.* (2010). The values were derived using the Hill/Howard (Hill & Howard, 1987) relationship in equation (3.9.26). Note the decrease in apparent goethite concentration (left axis) as the polymorphs of $Al(OH)_3$ (right axis) crystallize from solution.

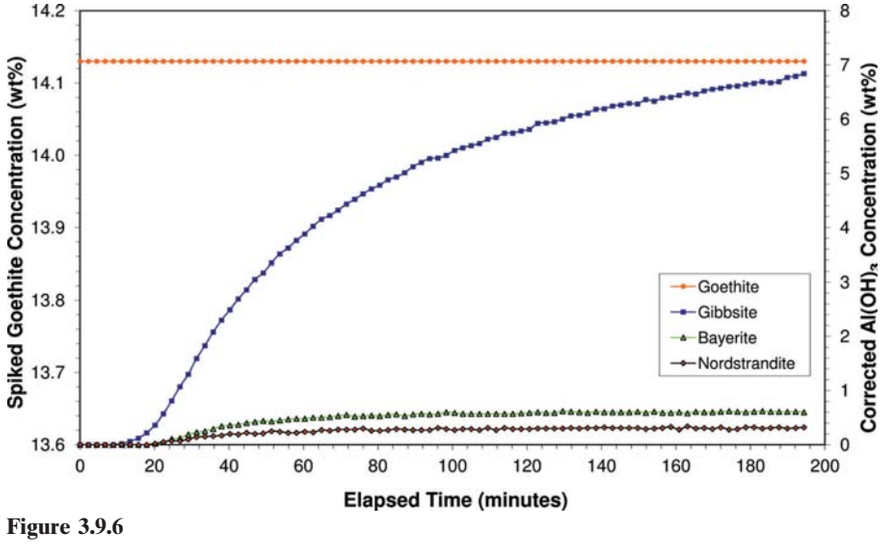

Figure 3.9.6
The results of QPA of the *in situ* XRD data collected during the seeding experiments of Webster *et al.* (2010).The values are absolute phase abundances derived using the internal standard relationship in equation (3.9.25).

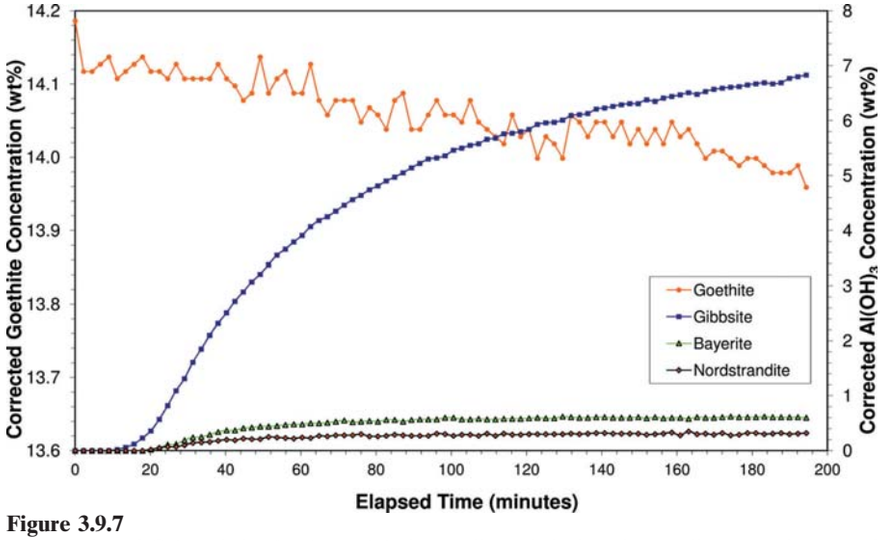

Figure 3.9.7
The results of QPA of the *in situ* XRD data collected during the seeding experiments of Webster *et al.* (2010). The values are absolute phase abundances derived using the external standard relationship in equation (3.9.22). Note the slight decrease in the goethite concentration (left axis) during the run.

for example, mineral exploration samples where a limited number of phases are present in a drill core but their abundance varies as a function of depth. In mineral processing or industrially based material manufacture, the goal is usually to control the system to minimize compositional variation in the product. The side effect of this is that the values of intensity in matrix **I** have too little variation, resulting in large errors in the derived values for *C*. In the limiting case, the system may become indeterminate with no unique solution available. To overcome this, forced or accidental changes to processing conditions may introduce sufficient compositional variation to stabilize the determination of the *C* values through equation (3.9.38). Alternatively, physical or chemical separation of selected components may be sufficient to provide the required compositional variation. Knudsen (1981) provides a detailed statistical analysis used in the determination of the errors in the phase constants.

While Zevin (Zevin & Kimmel, 1995) and Knudsen (1981) have demonstrated the application of this approach for single-peak methods, it is equally applicable if scale factors derived from whole-pattern fitting or Rietveld-based methods are used.

3.9.5.2. *Demonstration of the Zevin approach*

The sample 1 suite from the IUCr CPD round robin on QPA again provides an ideal platform for demonstrating the applicability of this method due to the wide variation of concentration of the constituent phases. A measure of intensity was derived using an hkl_phase (see Section 3.9.6) in which the peak positions were constrained to the space group and unit-cell parameters but the individual peak intensities were refined to empirical values using a pure sub-sample of each of the three phases. For the analysis of the samples, the relative peak intensities were fixed and an overall scale factor *S* for each phase in each sample (eight samples, three replicates, three phases), multiplied by the mass absorption coefficient calculated from the XRF-determined composition, was used as the measure of intensity. These $S\mu_m^*$ values then formed the intensity matrix **I** in equations (3.9.37) and (3.9.38) while all values in the vector **L** were assumed to be 1.0 (*i.e.* all samples were assumed to be fully crystalline). Microsoft Excel provides a useful platform for these calculations since it contains all of the matrix-manipulation functions required by equation (3.9.38). The determined values for *C* for the three phases are given in Table 3.9.3. The values in the C/C_{corundum} column should be compared with the values derived in Section 3.9.4.3 above.

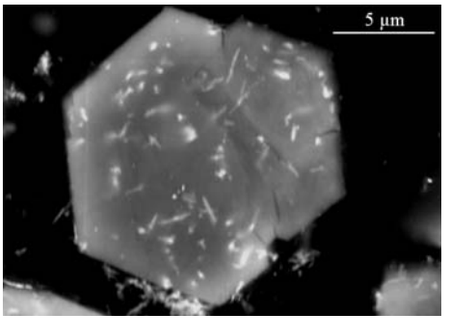

Figure 3.9.8
SEM image of $Al(OH)_3$ (grey hexagon) which has crystallized on goethite seed (light grey needles) (Webster *et al.*, 2010).

Application of these C values to the analysis of all samples *via* equation (3.9.34) yields the results given in Fig. 3.9.9. The results, displayed as bias from the known values, show that at all concentration ranges the analyses are within about ±1% of the weighed values. The important point to note here is that there has been *no prior calibration* conducted to obtain this result; the system is self-calibrating and has only relied on having a wide range of concentrations of the three phases in the sample suite. The only prior knowledge used in the analysis is (i) a measure of peak intensity embodied in the empirical phase scale factor and (ii) an estimate of μ_m^* for each sample calculated from the elemental composition.

3.9.5.3. *Experiment constant – a whole-sample approach*

Earlier discussion has noted that the experiment constant K used in equation (3.9.21) can be determined using (i) a standard pure phase or mixture measured separately from the measurement of the actual unknown mixture being analysed, or (ii) using a phase that is present in the sample in a known amount. However, in some cases, these approaches are not always effective in producing reliable values of K because the methodology assumes that the mass of sample contributing to the diffraction process is constant. While this condition is true for infinitely thick samples in Bragg–Brentano geometry, it is unlikely to be true for capillary or flat-plate samples in transmission geometry. In these cases, the sample thickness and packing density will have a significant influence on the amount of sample contributing to the diffraction process and hence on the observed intensity and the derived values of K. Therefore, a K value determined from one capillary sample is unlikely to be applicable to another capillary even though all other instrumental conditions remain the same. However, for *in situ* studies, a K value determined at the start of an experiment should remain valid as the analysis proceeds.

K can also be determined using the whole sample, rather than an individual phase. Since the determined value of K then applies equally to all phases in the sample, equation (3.9.21) can be summed over all analysed components thus:

$$\sum_{i=1}^{n} W_i = (\mu_m^*/K) \sum_{i=1}^{n} S_i(ZMV)_i. \qquad (3.9.39)$$

If the crystallinity of the sample is known (or can safely be assumed), then individual phase abundances are not required and K can be calculated from

$$K = \frac{\mu_m^* \sum_{i=1}^{n} S_i(ZMV)_i}{\sum_{i=1}^{n} W_i}, \qquad (3.9.40)$$

where $\sum W_i$ is the assumed crystallinity of the entire sample.

Table 3.9.3
Phase calibration constants for corundum, fluorite and zincite determined using the Zevin (Zevin & Kimmel, 1995) and Knudsen (Knudsen, 1981) method

The RIR values were derived earlier in this chapter.

Phase	C	C/C_{corundum}	RIR
Corundum	240.91	1.0	1.0
Fluorite	874.27	3.629	3.617
Zincite	1190.81	4.943	4.856

For a sample that is 100% crystalline and all components included in the analysis, then the denominator is unity and K is simply the sum of the product of the scale factors and their respective ZMV's multiplied by the mass absorption coefficient of the entire sample.

For *in situ* studies where a reaction or process is examined dynamically, sealed capillary sample geometry is frequently used. In this environment, the *chemical* composition of the capillary contents will not change during the course of the reaction even though individual phases may be undergoing transformation. Equation (3.9.40) can be further simplified since the overall sample mass absorption coefficient remains constant throughout the reaction and can therefore be deleted and its effect incorporated into K.

This whole-sample approach to the determination of K is also useful in systems where there are residual errors that may not be evident when equation (3.9.21) is used with the concentration of a single phase. By way of demonstration, the sample 1 suite from the IUCr CPD round robin on QPA has been used to calculate K in two distinct ways:

(1) *Phase specific*: Three replicate measurements of the eight mixtures were analysed using a Rietveld-based surface-analysis approach (Stinton & Evans, 2007). This approach refines a single model to all data sets in the suite simultaneously allowing parameters that are common to all samples to be determined with a greater degree of certainty. Since the sample suite contains corundum, fluorite and zincite in a wide range of concentrations, application of a rearranged equation (3.9.21) using the refined scale factors results in 72 separate determinations of K. The value of μ_m^* for each sample was derived from XRF-determined compositions using equation (3.9.5), while the values for W_i were taken from the known weight additions.

(2) *Whole sample*: Equation (3.9.40) was applied to each of the 24 data sets (*i.e.* three replicates each of the eight samples) assuming (i) that all phases were known and fully crystalline, *i.e.* $\sum W_i = 1$; and (ii) μ_m^* for each sample was derived in the manner described above.

Fig. 3.9.10 shows the 72 individual determinations of K from the phase-specific method as a function of known phase concentration. At high concentrations, the values for K derived from each of the three phases are similar indicating that, for effectively pure phase samples, the approach embodied in equation (3.9.21) is valid. However, if K is determined using the known concentration of a single phase at a lower concentration in a multiphase sample, then residual errors in the measurement of pattern intensity serve to reduce its accuracy. At lower concentrations of corundum, there is a systematic increase in the determined value of K resulting from a small microabsorption effect present in these samples. Since corundum has the lowest mass absorption coefficient of the three phases in this system its intensity, and hence Rietveld scale factor, is slightly

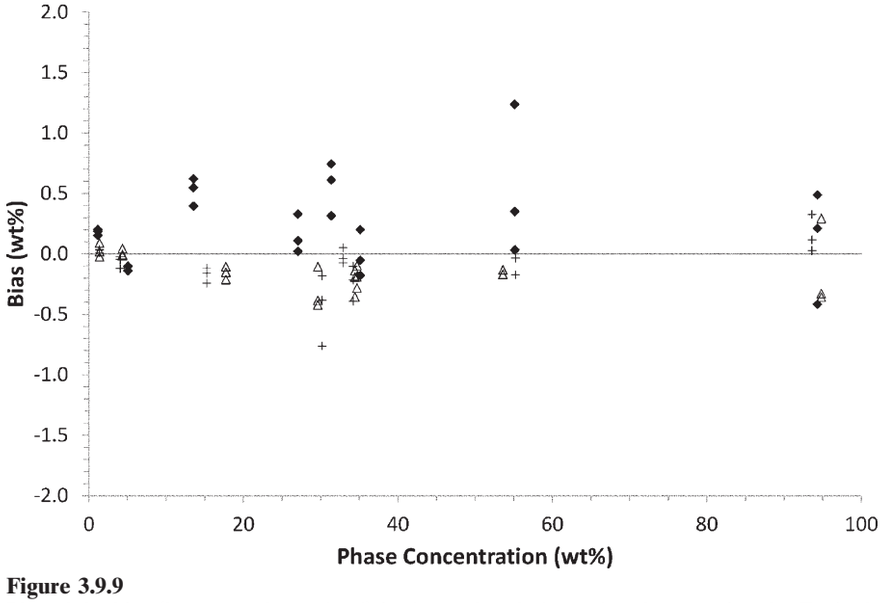

Figure 3.9.9
Plot of the bias (known − determined) in the analysed phase abundances using the Zevin & Kimmel (1995) approach for corundum (black diamonds), fluorite (open triangles) and zincite (crosses). The 72 determinations derive from three replicates of eight mixtures containing three phases each.

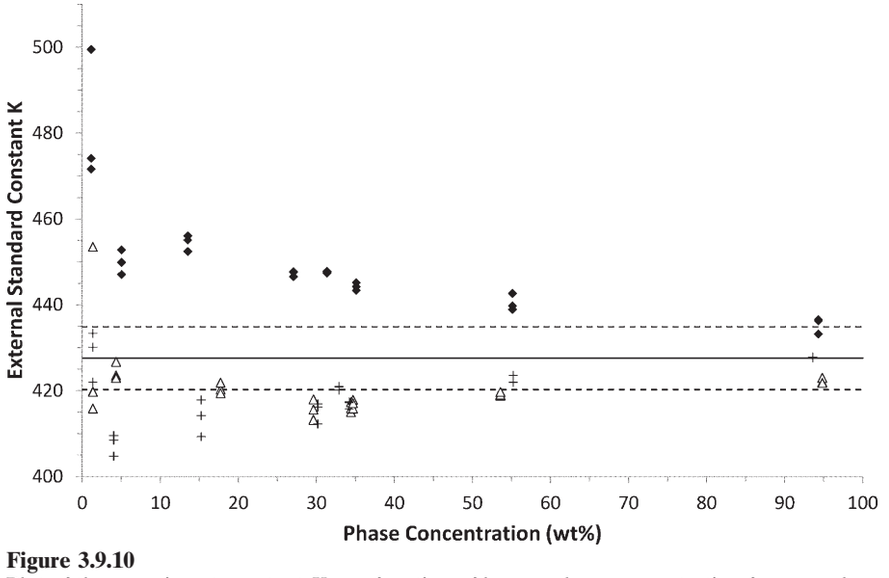

Figure 3.9.10
Plot of the experiment constant K as a function of known phase concentration for corundum (closed diamonds), fluorite (open triangles) and zincite (crosses) using the phase-specific method. The 72 determinations derive from three replicates of eight mixtures containing each of the three phases. The solid line is the mean of 24 values determined using the whole-sample approach. The dashed lines represent ±2 standard deviations about this mean.

overestimated relative to the fluorite and zincite. This results in an overestimation of the value of K relative to an ideal sample; the magnitude of this difference is about 5% relative. Use of these values for subsequent analysis will result in an underestimation of phase concentrations using equation (3.9.21). The converse is true if fluorite or zincite is used to determine K.

However, if the whole-sample approach embodied in equation (3.9.40) is used for the determination of K, these residual sample-related aberrations can be eliminated; the results of the determination of 24 values of K using this approach are also included in Fig. 3.9.10. The mean of all 24 determinations is 427.6 (3.7) representing a relative error of <0.8%. The important point to note here is that knowledge of the individual phase concentrations is not needed; the only assumption needed relates to the total crystallinity of each sample.

For *in situ* studies, using equation (3.9.40) to calculate K at each step i in the reaction (defined as K_i) can be useful in deriving details of the reaction mechanism. If K_i increases as the reaction progresses, this may be indicative of increasing crystallinity in the sample. Reductions in K_i during the reaction may point to the formation of intermediate amorphous material or unidentified crystalline components, the total concentration of which can be readily calculated using

$$\mathrm{wt\%}_{\mathrm{amorphous}} = 100\left(1 - \frac{K_i}{K}\right). \qquad (3.9.41)$$

Application of this can be demonstrated using sample 3 from the QPA round robin (Scarlett *et al.*, 2002), as it contains the same three crystalline phases as the sample 1 suite with the addition of 29.47 wt% amorphous silica flour. Calculation of K_i for sample 3, based only on the three crystalline phases, results in a value of 301.8. Substituting this into equation (3.9.41) along with the previously determined value of K (427.6) gives a measured amorphous content of 29.42 wt% – this is in good agreement with the known weighed amount. The important point to note here is that the data for sample 3 were collected at the same time, and under the same instrumental conditions, as for sample 1, which ensured that the true value of K was the same for all data.

3.9.6. Quantification of phases with partial or no known crystal structures

While the Rietveld-based methods described in Section 3.9.3.6 work for well ordered phases with known crystal structures, they are limited when published structure data do not accurately represent the phase actually present in the sample, are incomplete or do not exist. Poor agreement with published structure data is a common occurrence in mineralogical research where disorder exists and observed diffraction data deviate significantly from the ideal; this situation occurs with many of the clay minerals. The issue of incomplete or non-existent structure data can occur in almost any area where new materials are either synthesized or discovered. The growing demand for the analysis of materials from the nanotechnology community, where phases are at the boundary of what can be considered crystalline, serves to further highlight these limitations. Recent developments in diffraction methods have sought to address these issues and have used approaches that include the development of calibrated models or, where appropriate, the extension of existing structure data to incorporate systematic disorder such as stacking faults in clay minerals.

3.9.6.1. *Use of calibrated models*

Calibrated models are generally developed in one of two ways. The first (which uses what is referred to hereafter as an

hkl_phase) is obtained *via* the use of partial structure information. Here the peak positions are constrained by a unit cell and space group but the relative intensities, in the absence of atom types and locations in the unit cell, are determined empirically from a pure sample or one where the phase is present in a mixture at a known concentration. The second method involves the use of a discrete set of peaks whose positions, intensities, width and shape are all determined empirically. Once determined using a standard sample, this group of peaks may then be scaled as a single unit and is referred to hereafter as a peaks_phase.

The software *SIROQUANT* (Taylor & Rui, 1992) employs the simultaneous use of observed and calculated standard profiles within the framework of the Rietveld method. It draws on a library of structures that are stored as lists of reflections and intensities (hkl files). These are calculated on a cycle-by-cycle basis for well described crystalline materials but are read directly from the hkl files for poorly defined materials such as clay minerals. This method still requires some knowledge of the crystal chemistry of all phases involved and that they be included within the programme's database. By the inclusion of reflection information in this way some aberrations such as preferred orientation may be allowed for. This approach to clay mineralogy also provides for the refinement of two sets of halfwidth parameters in order to model the co-existing sharp and broad reflections generated by such minerals.

A subsequent development of the whole-pattern approach is the 'partial or no known crystal structure' (PONKCS) method (Scarlett & Madsen, 2006). This method operates within the framework of the Rietveld method but replaces the traditional crystal structure of the phases in question with an empirical set of peaks (either as an hkl_phase or a peaks_phase). These can then be scaled as a single unit in the course of refinement in similar fashion to the set of structure factors derived from a crystal structure. Since the full structure information is not available, it is not possible to calculate the *ZMV* phase constant normally required for quantification *via* equation (3.9.26) (Hill & Howard, 1987); hence, an empirical value must be derived through calibration.

3.9.6.1.1. *Generation of calibrated PONKCS models*

The generation of a suitable PONKCS model requires that:

(1) The unknown phase is available as either a pure specimen or as a component of a mixture where its abundance is known (in some instances, this may be achieved by other means, such as the measurement of bulk and/or microchemical composition.)

(2) The unknown phase does not vary considerably from the material used to derive the relative intensities of the model. Preferred orientation and other sample-related effects may be compensated for based upon an indexed diffraction pattern.

The initial step in the generation of a PONKCS model is to describe the contribution to the diffraction pattern of the phase with a series of peaks. If the phase of interest has been indexed, the Le Bail or Pawley methods (see Chapter 3.5) can be used to constrain peak positions to the space group and unit-cell parameters while the individual reflection intensities are allowed to vary to best match the observed peaks (*i.e.* an hkl_phase). If the phase has not been indexed, a series of unrelated peaks can be refined using a standard material and scaled as a group during analysis (*i.e.* a peaks_phase). While this approach is effective in most cases, it restricts the refinable parameters that may be used in the treatment of systematic errors such as preferred orientation.

The next step is to calibrate the hkl_phase or peaks_phase and derive a 'phase constant' that is equivalent to the *ZMV* value in crystal-structure-based quantification. This is achieved by the preparation of a mixture in which there are known amounts W_α and W_s of the unknown and standard, respectively. Recalling equation (3.9.25), the ratio of the weight fractions is then given by

$$\frac{W_\alpha}{W_s} = \frac{S_\alpha (ZMV)_\alpha}{S_s (ZMV)_s}, \tag{3.9.42}$$

where S_α and S_s are the refined scale factors for the unknown and standard, respectively.

Rearrangement of equation (3.9.42) then provides the means for determining an empirical value of $(ZMV)_\alpha$, which is required for the calibration of a peaks_phase:

$$(ZMV)_\alpha = \frac{W_\alpha}{W_s}\frac{S_s}{S_\alpha}(ZMV)_s. \tag{3.9.43}$$

For an hkl_phase the value of V can be determined from the refined unit-cell parameters and hence can be removed from the phase constant resulting in

$$(ZM)_\alpha = \frac{W_\alpha}{W_s}\frac{S_s}{S_\alpha}\frac{(ZMV)_s}{V_\alpha}. \tag{3.9.44}$$

Unlike the *ZMV* value derived from the unit-cell contents of a crystal structure, the phase constants derived using equations (3.9.43) and (3.9.44) have no physical meaning, since they have been derived by empirical measurement. For an hkl_phase, a more physically meaningful value of *ZM* can be obtained by deriving the true unit-cell mass from the measured phase density according to

$$(ZM)_{\alpha(\text{true})} = \frac{\rho_\alpha V_\alpha}{1.6604}. \tag{3.9.45}$$

The empirical 'structure factor' values in the hkl_phase could then be scaled according to the relation $ZM_{\alpha(\text{true})}/ZM_\alpha$, making them approximate 'real' structure factors for the material. Note that this final step is not necessary for quantification, but may make the method more generally applicable.

3.9.6.1.2. *Application of the model*

The PONKCS method is applicable to any mixture in which there are one or more phases that are not fully characterized crystallographically, including essentially amorphous material, provided appropriate calibration samples can be obtained. In the mineralogical context, it may not be possible to obtain pure phase specimens typical of those found in the bulk mixtures, but it may be possible to concentrate them to a point where they can be used. Methods of achieving this may include gravity or magnetic separation, or selective chemical dissolution.

The original paper describing this method (Scarlett & Madsen, 2006) gives a detailed example based upon sample 1 from the IUCr CPD round robin on QPA (Madsen *et al.*, 2001; Scarlett *et al.*, 2002). There, corundum was regarded as the unknown phase, fluorite as an impurity of known crystal structure and zincite a standard material added at known weight fraction. In the same paper, there is a more realistic example regarding the poorly ordered clay mineral nontronite, which is of commercial significance but difficult to quantify *via* traditional structure-based Rietveld methodology. Further details regarding quantification of this mineral *via* the PONKCS method is given in articles detailing

its importance in low-grade nickel laterite ores (Scarlett *et al.*, 2008; Wang *et al.*, 2011).

A calibration-based method such as PONKCS may also find increasing application with phases that have a known crystal structure. It has the greatest potential for accuracy, as the calibration process may obviate residual aberrations in the data such as microabsorption. Assuming that the sample suite has the same absorption characteristics as that used for calibration, such aberrations will be included in the calibration function and require no further correction during the sample analysis. This is a realistic scenario for routine analyses in industries as diverse as mineral processing, cement production and pharmaceutical production.

3.9.6.2. *Modelling of structural disorder*

One major challenge for QPA is the treatment of stacking disorder. An alternative to the use of calibrated models is to develop extended structure models that more effectively represent the phases present in the sample than the simple structure models. Stacking disorder occurs in layered structures where long-range order is present within the layers but there is only partial or even no relationship from one layer to another. It is a commonly occurring type of microstructure and is of great interest in various fields including mineralogy and material science.

The most common types of stacking faults in lamellar structures are:

(i) translational stacking faults, characterized by well defined translation vectors between successive layers;
(ii) rotational stacking faults, characterized by irregular but well defined rotation of adjacent layers in a stack; and
(iii) random stacking faults (turbostratic stacking), where there is no registry from one layer to another. This can be readily visualized as a stack of playing cards lying flat on top of each other but with no alignment between the edges (Fig. 3.9.11).

Mixed-layer (interstratified) systems contain different types of layers in a single stack, hence it is necessary to distinguish these from the types above. In this case, the layer types have different basal spacings and atomic coordinates (for example, illite–smectite interstratifications; Reynolds & Hower, 1970). Combinations of several of these types of disorder frequently occur in natural clay minerals. Intricate structural analysis using modelling techniques can give a reliable picture of the disorder of selected pure clay minerals, but such information is difficult to obtain from multiphase samples. Therefore, the type and degree of disorder of the components in natural rocks is one of the major unknowns when starting a quantitative analysis of such samples. The field of clay mineralogy represents a discipline where QPA has a long tradition, but has struggled with issues arising from a wide variety of disorder types. This complexity has led practitioners away from the use of crystallographic models and encouraged modification of the classical methods of quantitative analysis to incorporate empirical, calibration-based techniques such as those described earlier in this section.

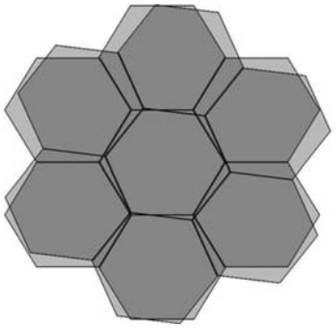

Figure 3.9.11
Turbostratic disorder, illustrated by the stacking of two hexagonal layers rotated by 7°.

An alternative approach is the application of a robust mathematical description of the observed features in the diffraction pattern, thus minimizing their impact on the QPA. In QPA, the existence of disorder contributes to inaccuracy through line broadening and shifting, which results in difficulties in the extraction of integral intensities or scale factors. A range of tools for the modelling of diffraction patterns of disordered layer structures has existed since the middle of the last century (Hendricks & Teller, 1942; Warren, 1941); these have been summarized by Drits & Tchoubar (1990).

In clay mineralogy, highly oriented samples are used for phase identification and characterization. One-dimensional diffraction patterns are collected initially from these, commonly air-dried, oriented samples and contain the information along **c*** that is characteristic of the type, composition and sequence of the layers comprising the clay. Based on this information, the clay minerals are classified into layer types, a classification which is a precursor to more precise identification of mineral species. Diffraction patterns are often collected again following various treatments of the oriented samples (*e.g.* solvation with ethylene glycol, heating to predetermined temperatures for specified times, wetting and drying cycles). Changes in peak positions, shapes and intensities between treatments are also diagnostic for identification of the clay mineral type present.

From a mathematical point of view, the one-dimensional calculation of intensities is much less laborious than a three-dimensional one, because only z coordinates are used and a–b translations and rotations are not considered. In 1985 Reynolds introduced the software package *NEWMOD* for the simulation of one-dimensional diffraction patterns for the study of interstratified systems of two clay minerals (Reynolds, 1985). This simulation was based upon a suite of parameters including instrumental, chemical and structural factors, and has been widely applied to the QPA of interstratified clays *via* the 'pattern-mixing' approach. An updated version (*NEWMOD+*; Yuan & Bish, 2010) has since been developed that incorporates improvements in clay-structure modelling, an improved GUI and the calculation of various fitting parameters that improve the operator's ability to estimate the quality of the profile fit.

The principal drawback of one-dimensional pattern approaches to QPA is that they are limited to the quantification of the ratio of layered structures only. Other minerals within the sample cannot be quantified at the same time. The degree of preferred orientation achieved in the oriented specimens may also differ between the mineral species present depending upon the method of sample preparation (Lippmann, 1970; Taylor & Norrish, 1966; Zevin & Viaene, 1990). This will affect the intensities of the observed peaks, which in turn affects the modelling of the relative proportions of the constituent minerals (Dohrmann *et al.*, 2009; Reynolds, 1989). Therefore, the quantification of minerals from severely oriented samples such as these is frequently inaccurate, as existing correction models are unable to describe the intensity aberrations adequately (Reynolds, 1989).

Quantification of clay minerals within multiphase specimens requires the modelling of the three-dimensional pattern of the randomly ordered clay. There are a number of approaches

incorporated in various software packages for the calculation of these three-dimensional diffraction patterns of disordered structures. *WILDFIRE* (Reynolds, 1994) calculates three-dimensional diffraction patterns of randomly oriented illite and illite–smectite powders with various types and quantities of rotational disorder. This is limited, however, to specific mineral types (the procedure has provided much information about the structural disorder of illite, for example) and is computationally demanding. Another approach is the general recursive method of Treacy *et al.* (1991), which simulates diffraction effects from any crystal with stacking disorder. This uses the intensity calculations of Hendricks & Teller (1942) and Cowley (1976) along with Michalski's recurrence relations describing disorder (Michalski, 1988; Michalski *et al.*, 1988). The calculation process for this method is less time consuming than that of *WILDFIRE*, but has the drawback of requiring the user to define the complete stacking sequence including stacking-transition probabilities and interlayer vectors. The original software for this method, *DIFFAX* (Treacy *et al.*, 1991), was extended by a refinement algorithm to *DIFFAX+* (Leoni *et al.*, 2004) and *FAULTS* (Casas-Cabanas *et al.*, 2006), but multiphase analysis is not possible within either package.

The application of Rietveld-based methods is widespread with many industrial applications, but their application to samples containing disordered materials is not yet routine. As the classical Rietveld method is based on the calculation of intensity for discrete reflections, the question of how the diffraction patterns of disordered phases may be modelled arises.

In principle, every atomic arrangement can be described in the space group *P*1 if the cell parameters are sufficiently large and a reflection-intensity calculation using the Rietveld method could then be performed. But the absence of symmetry in such 'large cell' models makes them inflexible, and parameters describing probabilities of translational and rotational stacking faults and layer-type stacking may not be directly included and refined. Nevertheless, some applications of such externally generated, large-cell structures in Rietveld phase analysis have been published; for example the phase analysis of montmorillonite (Gualtieri *et al.*, 2001).

The use of small, ideal cells in a traditional Rietveld approach for the calculation of diffraction patterns is hampered by the fact that the number of reflections generated by such models is insufficient to fit the asymmetric peak shapes of disordered layer structures. Standard anisotropic line-broadening models exist, such as ellipsoids (Le Bail & Jouanneaux, 1997), spherical harmonics (Popa, 1998) or the distribution of lattice metric parameters (Stephens, 1999), but these are typically unable to fit the patterns of disordered layered structures. They may also become unstable when physically unrealistic parameters are introduced, such as higher-order spherical harmonics. The application of such standard broadening models to clay minerals has therefore not proved successful.

Other Rietveld-based methods attempt to approximate the diffraction features of disordered layered materials by empirical enhancement of the number of reflections. The simplest method is the splitting of the reflections of a traditional cell into two or three separate reflections that can be separately broadened and shifted, following prescribed rules (Bergmann & Kleeberg, 1998). In this way, the broadening of special classes of peaks, for example reflections with $k \neq 3n$, can be modelled. This method is particularly suitable for structures showing well defined stacking faults, such as **b**/3 translations or multiples of 120° rotations. However, when structures show more complex disorder, such as turbostratic stacking, simple geometric dependencies of broadening and shifting are not sufficient to approximate their diffraction patterns.

Turbostratically disordered structures can be depicted in reciprocal space as infinite rods perpendicular to the *ab* plane and parallel to $\mathbf{c}^*$; see Fig. 3.9.12 (Ufer *et al.*, 2004). The diffraction features from such disordered materials consist of two-dimensional asymmetric bands, as can be observed typically for smectites and some other clay minerals (Brindley, 1980). One method for approximating the diffraction effects along the reciprocal-lattice rods within the Rietveld method is *via* the 'single-layer' approach (Ufer *et al.*, 2004). Here, a single layer is placed in a cell elongated along $\mathbf{c}^*$, which is effectively a 'supercell'. In doing this, an enhanced number of discrete lattice points are generated along the rods, according to the factor of elongation of the cell. This elongation generates a continuous distribution of additional *hkl* positions on the reciprocal rods. The inclusion of only a single layer in the supercell destroys periodicity, which is lacking in turbostratically disordered structures. By treating the pseudo-peaks of the supercell in the same manner as other structures within the Rietveld method (*i.e.*, introducing additional broadening, scaling the intensity) and separately calculating the peaks of the 00*l* series, the patterns of turbostratic structures like smectites can be reliably fitted. The model generated in this fashion can be used directly in phase quantification (Ufer, Kleeberg *et al.*, 2008; Ufer, Stanjek *et al.*, 2008).

However, this approach is limited to the turbostratic case. Moreover, the basal 00*l* series points are conventionally calculated, assuming rational diffraction from constant basal spacings in the stack. So the method cannot be applied to mixed-layered structures.

In order to overcome this limitation, Ufer *et al.* (Ufer, Kleeberg *et al.*, 2008; Ufer *et al.*, 2012) combined the recursive calculation method of Treacy *et al.* (1991) and the supercell approach in the structure-description code of the Rietveld software *BGMN* (Bergmann *et al.*, 1998). In this method a supercell is used to generate numerous discrete *hkl* spots along $\mathbf{c}^*$, but the partial structure factors are calculated by the recursive algorithm. This allows the refinement of structural parameters of mixed-layered structures and simultaneous Rietveld QPA to be performed (Ufer *et al.*, 2012). A broader introduction of such models in Rietveld phase analysis can be expected with the

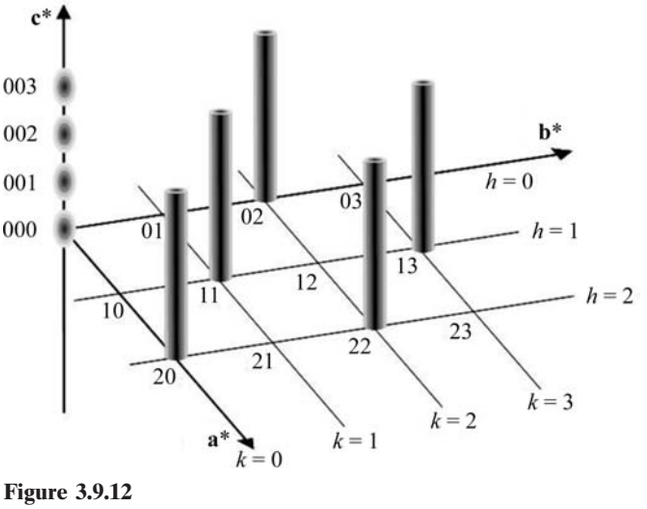

Figure 3.9.12
Section of the reciprocal lattice of a turbostratically disordered pseudo-hexagonal *C*-centred structure.

development of reliable structure models and enhanced computational power (Coelho *et al.*, 2016, 2015; Bette *et al.*, 2015).

3.9.6.3. *Quantitative determination of amorphous material*

Traditionally, most activity in diffraction-based QPA has been concerned with the assessment of the crystalline components. However, all materials possess a non-diffracting surface layer with some degree of disorder or contain some surface reaction products and adsorbed species. While such a layer can easily account for ∼1 wt% of the entire sample in a finely divided solid, the fraction of this surface layer will increase as the particle size decreases (Cline *et al.*, 2011). In addition, some materials can contain separate phases that may be amorphous or at least poorly crystalline. The advent of nanotechnology has served to further blur the boundaries between what is defined by powder XRD as crystalline or amorphous.

During *in situ* studies, some phases undergo transformations *via* amorphous intermediate components; the presence of these phases has the potential to influence our understanding of reaction mechanisms. Given the potential for these amorphous components to influence bulk-material properties, the need to quantify them is an increasingly important issue for analysts using diffraction-based methods. Many of the traditional phase-quantification techniques described in this chapter fail to take into account the occurrence of amorphous material in the sample and, without careful attention by the analyst, its presence may remain undetected.

Madsen *et al.* (2011) recently reviewed a range of techniques for the determination of amorphous content and assessed their applicability for various analytical situations. The study used both single-peak and whole-pattern methodology and applied it in two distinct ways.

(1) The first method used an indirect approach; the crystalline components were quantified and put onto an absolute scale using either an internal- or external-standard method. The amorphous content was then determined by subtracting the sum of the absolute weight fractions of the crystalline components from unity.
(2) The second method used a direct approach; it relied on being able to 'see' the amorphous contribution in the diffraction and being able to obtain an estimate of its intensity during analysis (Fig. 3.9.13). Intensity contributions of amorphous phases are not always evident in the diffraction pattern, especially at low concentrations. Even when their presence is apparent, it can be difficult to resolve their contribution from other components of the diffraction pattern such as pattern background. However, once an intensity estimate is obtained, and an appropriate calibration constant derived, the amorphous phase can be included in the analysis along with the crystalline components.

In general, for the determination of amorphous material the problem will dictate the method(s) used. All methods discussed in the study of Madsen *et al.* (2011) are, in principle, capable of determining the concentration of amorphous material in mixtures with similar levels of accuracy and precision as is possible for crystalline phases (down to ∼1% absolute or better). The limitations are similar to those for the QPA of crystalline phases, and are dictated by sample properties and the analytical techniques used.

A summary of the recommendations resulting from the study include:

(1) Where the intensity contribution of the amorphous content to the diffraction pattern is not evident, one of the indirect methods (internal or external standard) should be used. For indirect methods, any errors in the analysis of the crystalline phases will decrease the overall accuracy attainable since the amorphous phase abundance is determined by difference.
(2) Where intensity contributions of amorphous phases are evident in the diffraction pattern, any method based on the direct modelling of the amorphous component provides improved accuracy relative to the indirect methods.
(3) Calibration-based methods usually have the potential to achieve the highest accuracy, as residual aberrations in the data, such as microabsorption, are included in the calibration function. Caution is advised here as the magnitudes of these residual errors may change with different sample suites, and so a calibration function derived for one sample suite may not be generally applicable.
(4) A sample of pure amorphous material, or a sample where the amorphous content is high and its concentration known, is normally required to establish an accurate model for the direct methods.

Some materials contain more than one amorphous phase and there may be a desire to quantify these separately rather than as a group. This provides a significant challenge since their broad diffraction patterns will be highly overlapped, thus leading to a high degree of correlation during analysis. However, Williams *et al.* (2011) have demonstrated that, with careful experimentation and data analysis, it is possible to provide QPA for two poorly crystalline components in geopolymers.

Phase abundances reported in the literature are often provided in a manner that suggests they are absolute values. Where no specific allowance for amorphous content has been made and reported, it is better to assume that the reported phase abundances are correct relative to one another, but may be overestimated in an absolute sense. Therefore, standard practice in QPA should be to use methodology which produces *absolute* rather than *relative* phase abundances. Any positive difference between unity and the sum of the absolute weight fractions will

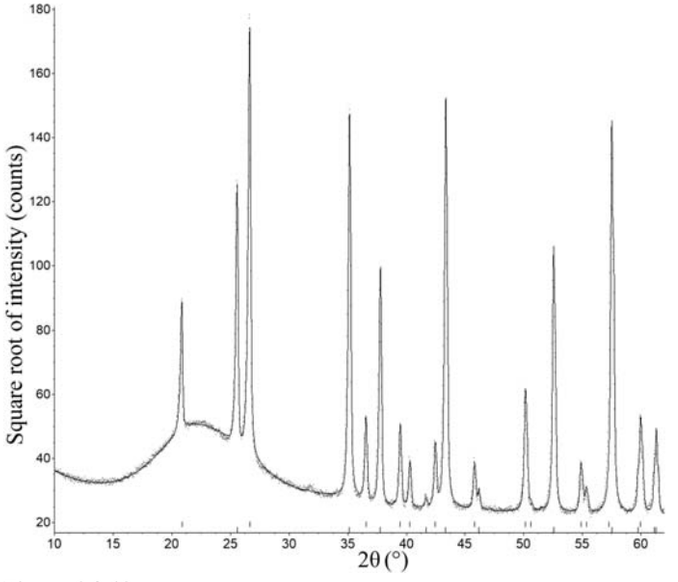

Figure 3.9.13
Output of Rietveld refinement of XRD data (Cu $K\alpha$ radiation) for a synthetic sample containing a mixture crystalline and amorphous phases. The observed data are represented as grey dots and the calculated pattern as the solid black line overlaying them. The broad peak centred at ∼22° 2θ is due to amorphous silica flour. The rows of tick marks at the bottom represent the positions of the Bragg reflections for quartz (upper) and corundum (lower).

alert the analyst to the presence of non-analysed material in the sample.

3.9.7. QPA from *in situ* experimentation

In situ analysis is a growth area in the field of powder diffraction (Ehrenberg *et al.*, 2013) and is dealt with in depth elsewhere in this volume (see Chapter 2.9). The technique is unparalleled in providing information about reaction mechanisms and kinetics under simulated operational conditions and without the artefacts potentially associated with post-mortem sampling or *ex situ* methods.

An *in situ* experiment collects dynamic, time-resolved data, which present unique challenges for QPA. The phase assemblages formed in such experiments may be quite complex and change dramatically over the course of the experiment. In addition, the data are generally of lower quality than those collected for *ex situ* samples at ambient conditions. This may be due to poor counting statistics resulting from the rapid counting times needed to follow various phase transitions. Data for *in situ* studies are often collected using area detectors, some of which are not photon-counting devices. Care should be taken in the error propagation and hence the weighting used during data analysis.

The data quality may also be affected by components in the sample chamber that are required in order to achieve the environmental conditions (temperature, pressure, solution or gaseous atmosphere, and so on) necessary for the experiment: these components may either attenuate the incident and diffracted beams or contribute features to the pattern resulting from scattering of the beam.

One very important issue that arises from *in situ* studies is the large number of data sets generated. The rapid counting times available at modern synchrotron and neutron facilities mean that hundreds or thousands of diffraction patterns can be collected over the duration of the *in situ* experiment.

3.9.7.1. *Data analysis*

There are usually a series of steps involved in the analysis of *in situ* diffraction data. Given the large number of data sets collected, it is generally not practicable to undertake detailed analysis of every pattern individually. Since any changes to the component phases are transitions generally observed in a sequence of patterns, data analysis focused on extracting QPA could be undertaken using the following steps:

(1) Cluster the data into a number of groups necessary to describe the major phase regions present during the reaction. This can be achieved (i) visually, using software that allows the plotting of three-dimensional data sets of the type shown in Fig. 3.9.14, or (ii) through the use of automatic clustering algorithms using, for example, principal-component analysis.

(2) Select the 'most typical' pattern of each cluster as well as the two 'least typical' patterns at the extreme ends of the cluster. These patterns are often identified by clustering software based on the statistical similarity between patterns in the cluster.

(3) Identify the phases present in each cluster using the most typical pattern. This is not always a trivial task since (i) new phases that are not currently present in databases may have been generated; (ii) effects such as thermal expansion or variation of chemical composition may have changed the peak positions so that search/match procedures are no longer successful; or (iii) impurity elements may have stabilized phases that are not expected from related phase-diagram studies.

(4) For the discussion here, it will be assumed that the quantification process will be *via* a whole-pattern method.
   (*a*) Develop appropriate (crystal structure or PONKCS) models for every phase observed within the data suite.
   (*b*) Optimize the pattern and phase-analysis parameters using the most typical pattern selected from each cluster.
   (*c*) Set the relevant parameter refinement limits using the least typical patterns. It is necessary to limit the range over which refined parameters can vary to avoid the return of physically unrealistic values.

(5) Owing to the large number of data sets, analysis for QPA will generally be approached as a batch process with limited refinement of structural parameters. This limitation on the total number of refinable parameters is necessary during batch processing in order to avoid instability in the refined values as the phases progress from major to minor concentration.

(6) Batch processing of data suites may be conducted in a variety of ways including:
   (*a*) Sequential refinement, beginning with either the first or final pattern of the suite and including all phases present in the entire suite. This methodology must be tempered by a means to either remove or severely restrict refinement of any phases that are not present in all patterns of the suite in order to avoid the reporting of 'false positives' where absent phases have been included. Some software packages allow phases to be removed from the analysis if their abundance is below a selected level or has an error that exceeds some predefined criteria (Bruker AXS, 2013).
   (*b*) Parametric Rietveld refinement (Stinton & Evans, 2007), where the entire suite of diffraction data is analysed simultaneously. Selected parameters are constrained to the applied external variable (*e.g.* temperature) with a function describing their evolution throughout the data sequence. For example, the unit-cell parameters for a phase can be constrained to vary according to their thermal coefficients of expansion. This method can bring stability to refined parameters and allows the refinement of noncrystallographic parameters such as temperature and reaction rate constants directly from the diffraction data. This methodology is particularly suited to relatively simple phase systems, but is difficult to develop for complex multiphase mineralogical systems.

(7) In selecting a model for use in QPA, it is highly recommended that one of the approaches that generate absolute phase abundances is used. Many reactions generate intermediate amorphous phases that convert to crystalline components later in the reaction. If relative phase abundances [such as those produced by the *ZMV* approach embodied in equation (3.9.26)] are used, the amounts of the crystalline phases will be overestimated and this will give misleading indications about the reaction mechanism and kinetics.

Whichever method is employed, it is always necessary to examine a sample of individual results as a test of veracity rather than just accepting the suite of numbers for parameter values and QPA resulting from batch processing.

The study of Webster *et al.* (2013) demonstrates many of these points by following the formation mechanisms of the iron-ore

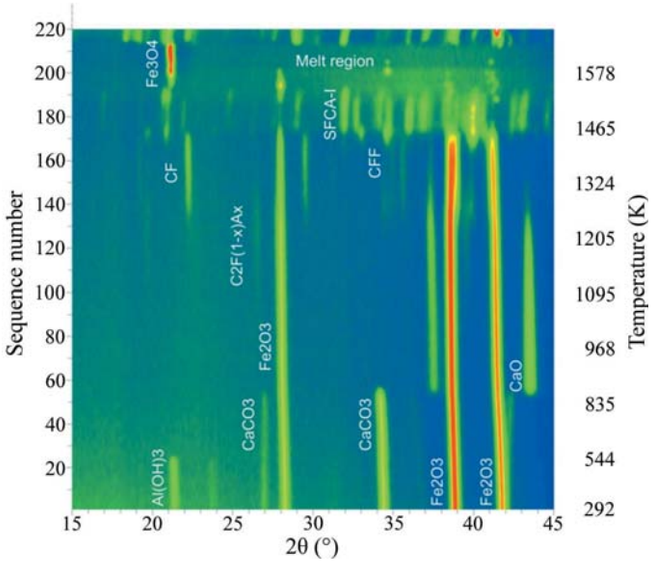

Figure 3.9.14
Raw *in situ* XRD data (Co $K\alpha$ radiation) collected during the synthesis of the iron-ore sinter bonding phase SFCA-I (Webster *et al.*, 2013). The data, collected as a function of heating temperature, are viewed down the intensity axis with red representing the highest intensity and blue the lowest intensity. The identified phases include gibbsite $Al(OH)_3$, calcite $CaCO_3$, haematite Fe_2O_3, lime CaO, calcium ferrites CF and CFF, calcium alumina-ferrite $C_2F_{1-x}A_x$, magnetite Fe_3O_4, and SFCA-I.

sinter bonding phase, SFCA-I, where SFCA = silico-ferrite of calcium and aluminium (Scarlett, Madsen *et al.*, 2004; Scarlett, Pownceby *et al.*, 2004; Webster *et al.*, 2013). The starting material, comprising a synthetic mixture of gibbsite, $Al(OH)_3$, haematite, Fe_2O_3, and calcite, $CaCO_3$, was heated to about 1573 K using an Anton Paar heating stage. The laboratory-based XRD data, collected using an Inel CPS120 diffractometer, are shown in Fig. 3.9.14, while the QPA results are shown in Fig. 3.9.15. Both figures show that there are several phase changes, including the formation of transient intermediate phases before the final production of SFCA.

In Fig. 3.9.15(*a*) the QPA results are derived using the Hill/Howard algorithm (Hill & Howard, 1987) in equation (3.9.26): this is the 'default' value reported by most Rietveld analysis software and normalizes the sum of the analysed components to 100 wt%. The apparent increase in haematite concentration at about 533 and 868 K results from the decomposition of gibbsite and calcite, respectively. There are no possible mechanisms in this system that could lead to an increase in haematite concentration at these temperatures; the reported increases are an artefact derived from normalizing the sum of all analysed phases to 100 wt%. Fig. 3.9.15(*b*) shows the correct result derived using the external-standard approach (O'Connor & Raven, 1988) embodied in equation (3.9.21), which has placed the values on an absolute scale. Fig. 3.9.15 demonstrates the importance of putting the derived phase abundances on an absolute scale for a realistic derivation of reaction mechanism and kinetics.

3.9.8. QPA using neutron diffraction data

One of the early papers detailing the application of the Rietveld method to quantitative phase analysis used neutron diffraction (ND) data (Hill & Howard, 1987). The reasons stated within this work define many of the advantages of neutrons over X-rays for diffraction in general and QPA in particular. One of the most significant advantages for QPA derives from the fact that neutrons interact weakly with matter, hence there is very little microabsorption with ND even in samples comprising a mixture of high- and low-atomic-number materials.

The high penetration capability of neutrons also enables the use of larger sample environments in *in situ* studies, thus enabling studies to be undertaken at, for example, higher pressures than would be possible with many X-ray sources. In addition, larger sample volumes can be investigated, which in turn produces better particle statistics and makes the technique less sensitive to grain size. It also makes ND a bulk technique in comparison with XRD, which is effectively surface-specific with a penetration depth of the order of microns or tens of microns.

The different strengths of ND and XRD mean that they can be exploited in combination to provide complementary information. For example, XRD generally has higher angular resolution and is therefore better at resolving small lattice distortions and heavily overlapped phases. However, the observed intensities in ND do not decrease as strongly with decreasing *d*-spacing. This results in ND providing more accurate determination of atomic displacement parameters and therefore the Rietveld scale factors; this then improves the accuracy of QPA derived from these scale factors (Madsen *et al.*, 2011).

Hill *et al.* (1991) have investigated the phase composition of Mg-PSZ (partially stabilized zirconia) using both ND and XRD. The surfaces of these materials were subjected to various treatments, which meant that they were no longer representative of the bulk. From the more highly penetrating ND data they obtained bulk properties including crystal structure and size and strain parameters of the components along with QPA. From XRD they were able to examine the surface of the samples to investigate the effects of surface grinding and polishing.

The majority of Rietveld-based QPA still relies on the use of accurate crystal structure models; consequently, it is of increasing importance that powder diffraction methods used for structure solution be robust and reliable. Combining laboratory or synchrotron XRD and ND has been shown to be of considerable benefit in the solution of complex structures *via* powder diffraction (Morris *et al.*, 1992). This joint-refinement approach has been used to determine the crystal structure of a component phase of Portland cement (De La Torre *et al.*, 2002) for subsequent use in Rietveld-based QPA.

One of the disadvantages of neutron sources is that they are much less accessible than laboratory X-ray sources and of much lower flux than either laboratory or synchrotron X-rays sources. In addition, larger samples are generally required; this is not always practical in the investigation of many materials.

In many phase systems, the presence of severe microabsorption in XRD data serves to limit the accuracy that can be obtained. The collection of ND data, where microabsorption is virtually absent, from selected samples provides more accurate QPA; selected ND-based values can therefore act as a benchmark for the more routine XRD-based studies.

3.9.9. QPA using energy-dispersive diffraction data

Energy-dispersive diffraction (EDD) involves the use of high-energy white-beam radiation, often from a synchrotron source. This provides very high penetration and is, therefore, ideal as a probe to examine the internal features of relatively large objects (Barnes *et al.*, 2000; Cernik *et al.*, 2011; Hall *et al.*, 1998, 2000). In an experimental arrangement such as that in Fig. 3.9.16, diffraction data can be measured by energy-dispersive detec-

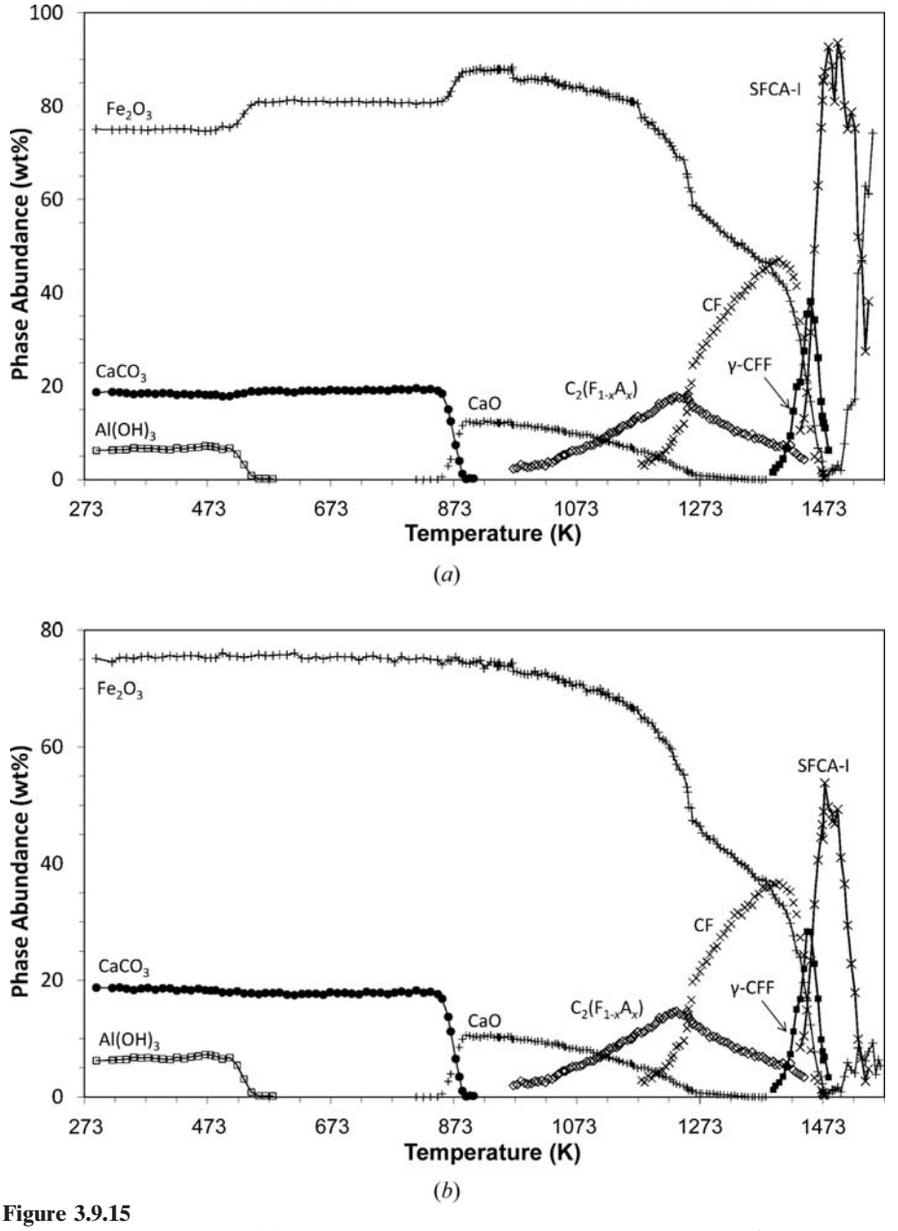

Figure 3.9.15
Results of Rietveld-based QPA of the *in situ* data sequence shown in Fig. 3.9.14 (Webster *et al.*, 2013). The relative phase abundances (upper) are derived using the Hill/Howard algorithm (Hill & Howard, 1987) in equation (3.9.26), while the absolute phase abundances (lower) have been derived from the external-standard approach (O'Connor & Raven, 1988) embodied in equation (3.9.21).

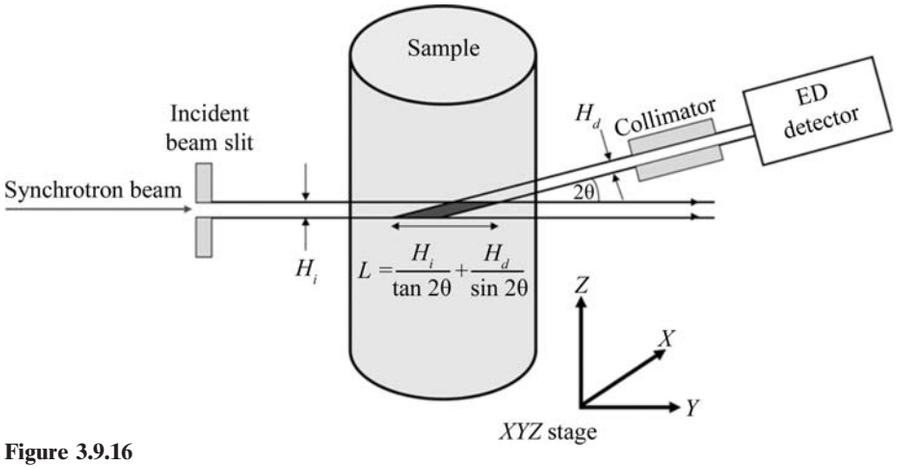

Figure 3.9.16
Basic experimental arrangement for energy-dispersive diffraction. The length of the active area or lozenge (dark grey region), L, is given by the function relating the incident- and diffracted-beam heights (H_i and H_d, respectively) and the angle of diffraction (2θ).

tors producing a spectrum of diffracted intensity as a function of energy.

Traditional angle-dispersive diffraction (ADD) satisfies Bragg's law by using a fixed wavelength and varying 2θ to map the d-spacings. In contrast, EDD data are collected directly on an energy scale at a constant 2θ and the energy is measured to map the d-spacings. This impinges upon the use of Rietveld methodology for QPA since, in contrast to ADD, the structure factors now vary as a function of energy. Energy is related to wavelength *via*

$$E\ (\text{keV}) = \frac{hc}{\lambda} \simeq \frac{12.395}{\lambda}, \qquad (3.9.46)$$

where E is the energy of the incident radiation in keV, h is Planck's constant, c is the speed of light and λ is the wavelength associated with that energy in ångstroms. Rearrangement of equation (3.9.46) and substitution for λ in Bragg's law enables the mapping of the measured energy scale to d-spacings:

$$E\ (\text{keV}) = \frac{6.197}{d \sin\theta}, \qquad (3.9.47)$$

where 2θ is the angle between the incident beam and the detector slit.

EDD data can be analysed using structureless profile-fitting methods such as those of Le Bail *et al.* (see Chapter 3.5) once the energy scale has been converted to a d-spacing scale (Frost & Fei, 1999; Larson & Von Dreele, 2004; Zhao *et al.*, 1997). If the distribution of intensities in the incident spectrum can be measured, it is possible to normalize the EDD data, correct for absorption and convert the pattern to an ADD form using a 'dummy' wavelength (Ballirano & Caminiti, 2001). Access to the incident spectrum, however, is not always possible, especially at synchrotron-radiation sources where the highly intense incident beam could damage the detector.

An alternative approach is to model the pattern directly on the energy scale *via* equation (3.9.47) (Rowles *et al.*, 2012; Scarlett *et al.*, 2009) and extract phase abundances using the methodologies described earlier in this chapter.

However, the major impediment to achieving this is the nonlinearity of the intensity distribution in the incident spectrum. This is due to (i) the nonlinear distribution of intensity as a function of energy in the incident beam, (ii) nonlinear detector responses (Bordas *et al.*, 1977) and (iii) absorption along the beam path (by the sample and air), which skews the energy distribution to the higher energies. This overall nonlinearity can be modelled empirically by functions such a lognormal

curve (Bordas *et al.*, 1977; Buras *et al.*, 1979) or by an expansion of a power function (Glazer *et al.*, 1978). Alternatively, it may be determined experimentally by the use of standards measured under the same conditions as the experiment (Scarlett *et al.*, 2009). This latter approach allows some separation of the contributions from the instrument and the sample, and allows some degrees of freedom in the refinement of sample-related parameters that may be of benefit in dynamic experiments. Other contributions to the diffraction pattern that must also be accounted for include any fluorescence peaks arising from the sample or shielding or collimators, and any detector escape peaks from both diffracted and fluorescence peaks. Fluorescence peak positions and relative intensities should be constant throughout the measurement and may therefore be modelled using a fixed 'peak group' whose overall intensity can be refined during analysis. Escape peaks can be accounted for by the inclusion of a second phase identical to the parent phase but with an independent scale factor and a constant energy offset determined by the nature of the detector (Rowles *et al.*, 2012).

Currently, few Rietveld software packages are capable of dealing directly with the differences between EDD and ADD, specifically (i) the variance of structure factors as a function of energy, (ii) the nonlinear distribution of intensity in the incident beam as a function of energy further modified by a nonlinear detector response, and (iii) the preferential absorption of lower-energy X-rays by the sample/air. *TOPAS* (Bruker AXS, 2013) embodies algorithms that allow the pattern to be modelled directly on the energy scale and also the inclusion of equations to account for intensity variations arising from the experimental conditions. This allows quantification from such data to be achieved directly using Rietveld-based crystal-structure modelling incorporating the Hill and Howard algorithm in equation (3.9.26) (Hill & Howard, 1987). The application of *TOPAS* to a complex EDD experiment investigating the changes to the anode during molten-salt electrochemistry conducted in molten $CaCl_2$ at about 1223 K has been described by Rowles *et al.* (2012) and Styles *et al.* (2012).

3.9.10. Improving accuracy

There are many factors that influence the accuracy and precision of QPA results where (i) accuracy is defined as the agreement between the analytical result and the true value, and (ii) precision is the agreement between results if the analysis is repeated under the same conditions. Precision may further be split into (i) repeatability, which is the agreement between repeated measurement and analysis of the same specimen, and (ii) reproducibility, which additionally includes re-preparation, measurement and analysis of the sample.

3.9.10.1. *Standard deviations and error estimates*

Determination of the actual accuracy of an analysis is not a trivial task in a standardless method. In fact, it cannot be achieved without recourse to another measure of the sample that does incorporate standards. Too often, analysts will report Rietveld errors calculated in the course of refinement as the errors in the final quantification. However, these numbers relate purely to the mathematical fit of the model and have no bearing on the accuracy of the quantification itself.

Consider, for example, a three-phase mixture of corundum, magnetite and zircon. Such a sample was presented as sample 4 in the IUCr CPD round robin on QPA (Scarlett *et al.*, 2002). Its components were chosen with the deliberate aim of creating a sample in which severe sample-related aberrations occur. Table 3.9.4 shows the weighed amounts of each component and the results of replicate analyses of three different sub-samples of this material.

Table 3.9.4
Comparison of errors generated during the analysis of XRD data (Cu $K\alpha$ radiation) from three sub-samples of sample 4 from the IUCr CPD round robin on QPA (Scarlett *et al.*, 2002)

The bias values are (measured − weighed) while the values denoted XRF are the phase abundances generated from elemental concentrations measured by X-ray fluorescence methods.

	Phase		
n = 3	Corundum	Magnetite	Zircon
Weighed	50.46	19.46	29.90
Mean XRD measured wt%	56.52	17.06	26.42
Mean of Rietveld errors	0.15	0.11	0.11
Standard deviation of measured wt%	0.63	0.41	0.35
Mean of bias	6.06	−2.58	−3.48
XRF	50.4(2)	19.6(1)	29.5(1)

It is apparent that the standard deviation of the mean abundances of the three replicates, which represents the expected precision in the analysis, is 3 to 4 times greater than the errors reported by the Rietveld software. The good level of fit achieved in conducting these analyses (evidenced by low R factors) could lead the analyst to conclude that the mean value ± the standard deviation of the mean is an adequate measure of the phase abundances and their errors.

However, both the Rietveld errors and the precision are at least an order of magnitude smaller than the bias. The large bias, in this case due to the presence of severe microabsorption, represents the true accuracy that can be achieved in this example. Unfortunately, there is nothing in the XRD data and Rietveld analysis process that indicates that there may be a problem. It is only when the QPA is compared with other estimates, in this case derived from XRF chemical-analysis results, that the problem becomes apparent. The analyst must take further steps to identify sample-preparation and/or data-collection protocols that may improve accuracy and, importantly, seek ways to verify the results.

3.9.10.2. *Minimizing systematic errors*

The fundamental measured quantities in a diffraction pattern are the integrated intensities of the observed peaks. The precision of these measurements can be improved by: (i) increasing the primary intensity of the diffractometer using optics or higher-power X-ray sources; (ii) using scanning linear detectors (see Chapter 2.1), which have multiple detector elements to collect individual intensities many times; these are then summed to achieve higher accumulated counts; (iii) increasing the number of counts accumulated at each step, that is increasing the step counting time T; and (iv) increasing the number of points, N, measured across the peak.

Often, the temptation is to collect data with large values of N and T to maximize counting statistics. However, the resulting increased precision is only useful up to the point where counting variance becomes negligible in relation to other sources of error; thereafter data-collection time is wasted. For example, if the sample is affected by the presence of severe sample-related

aberrations, the collection of highly precise data will not improve the accuracy of the resulting analysis significantly.

Therefore, the most important approach to improving the accuracy of an analysis is to eliminate the systematic errors. Given that the largest sources of error in QPA are experimental (Chung & Smith, 2000) and relate to sampling and specimen preparation, then this is the area on which the most careful attention needs to be focused. A detailed discussion of sample preparation and data-collection procedures is beyond the scope of this chapter but further details can be found in Chapter 2.10, and in Hill & Madsen (2002) and Buhrke *et al.* (1998).

3.9.10.3. *Minimizing sample-related errors*

3.9.10.3.1. *Crystallite-size issues*

Crystallite size is considered here as the length of a coherent scattering domain and should not be confused with the terms grain or particle size used frequently in powder diffraction to describe the macroscopic size of the components in the sample. The macroscopic size of the particle is somewhat irrelevant (as in ceramics or other solid pieces of samples) as long as the crystallites (or domains) that comprise the particle are (i) sufficiently small to ensure that there are enough crystallites contributing to the diffraction process (Smith, 1992) and (ii) randomly oriented, thus ensuring a true powder-average representation of intensities. However, for large domains or crystallites this assumption is usually not fulfilled and therefore it is necessary to reduce the crystallite size by reducing the size of the particles or grains that constitute the macroscopic objects of a powder.

Most issues in sample preparation are related to crystallite size and preferred orientation of the particles in the sample holder. For QPA a representative sampling of all possible orientations of crystallites with respect to the diffraction geometry is required. Rotation of the sample improves the particle statistics, since more crystallites can satisfy the diffraction condition (Elton & Salt, 1996).

Large-crystallite issues are easily detected using two-dimensional (2D) detectors, where the Debye rings show a 'spotty' intensity distribution. However, most QPA measurements are performed using 0D (point) or 1D (strip) detectors. The effect of large crystallites in a 1D pattern is that a few crystallites may contribute to irregularly high intensities for selected reflections. In the diffraction pattern, this situation is usually identified by intense reflections having a sharp peak profile compared with the surrounding peaks in the pattern. Furthermore, in a Rietveld refinement this situation is manifested by large intensity differences between the observed and calculated pattern that may not be associated with a particular crystallographic direction and hence to preferred orientation. Another way of detecting inhomogeneous crystallite distributions is to measure a series of scans from the same specimen at various rotation angles and comparing the relative peak intensities. It is worth noting that the push towards ever higher resolution in both laboratory and synchrotron instruments serves to further exacerbate the crystallite-size issue. This arises from the use of beams with decreased divergence, resulting in fewer crystallites likely to satisfy the diffraction condition.

There is no simple mathematical correction for large-crystallite issues and the effect is often misinterpreted in Rietveld refinement as preferred orientation. In this case, the correction would typically involve use of several directions for March–Dollase-type functions (Dollase, 1986) or an increasing order of spherical-harmonics coefficients (Ahtee *et al.*, 1989). In any case, this is an improper use of these corrections and the necessity to do so clearly points to deficiencies in the sample preparation and data-collection regime.

The best way to minimize the large-crystallite issue is to reduce the crystallite size through grinding of the sample. However, size-reduction methods need to be carefully assessed, since over-grinding can cause peak broadening due to (i) a decrease of long-range order and hence crystallite size and (ii) the introduction of microstrain (Hill & Madsen, 2002). The practical effect of peak broadening is increasing peak overlap, which may complicate the phase identification. For whole-pattern-based QPA, overgrinding is not as serious as long as it does not yield nanometre-sized particles or amorphous materials. This is because the integral intensity of the peaks is preserved. It should be noted that some phases can undergo transformation to other polymorphs or decompose to other phases during grinding (Hill & Madsen, 2002).

In practice, there is no generally applicable comminution strategy. For each material, a suitable milling device and grinding strategy needs to be identified. Inhomogeneous materials such as ores, concentrates and other mineralogical materials may have very different comminution properties for their constituents, leading to size fractionation during grinding. Large-crystallite issues are frequently observed for hard minerals (*e.g.* quartz, feldspar) while the grain size of soft minerals (*e.g.* talc) is reduced more rapidly.

A practical way of finding a best compromise for the milling conditions of a mixture may be the analysis of a series of samples of the same material where, for example, the grinding time is successively increased and the quantification results are compared. Fig. 3.9.17 shows the variation of analysed wt% with grinding time for two minerals: a stable result is eventually obtained.

There is a more extensive discussion of the impact of large-crystallite size on observed diffraction data (Smith, 1992) and ways to minimize its effect (Elton & Salt, 1996) in the published literature.

3.9.10.3.2. *Preferred orientation*

In order to generate peak intensities that accurately represent the intensity-weighted reciprocal lattice, the crystallites in the powder must not only be sufficient in number, but they must also be randomly oriented. In other words, each crystal orientation should have the same probability of diffracting. Preferred orientation can arise when particles align in the sample holder according to their morphology. This is most common with platy or

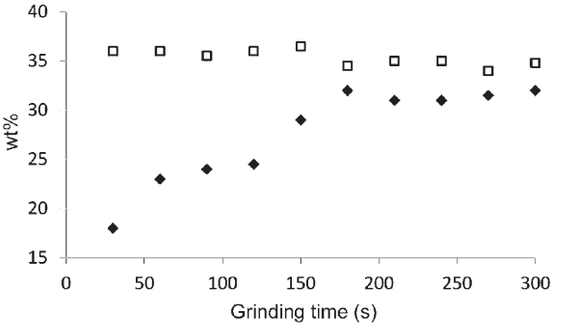

Figure 3.9.17
Variation of the magnetite (filled diamonds) and quartz (open squares) concentration of an iron-ore sample with grinding time. Stable conditions are obtained after about 180 s. Data courtesy ThyssenKrupp – Resource Technologies (Knorr & Bornefeld, 2013).

needle-like materials and the effect on the diffraction pattern is the observation of enhanced intensity along specific crystallographic directions with a subsequent decrease of intensity along other directions.

A number of sample-presentation methods can be used to minimize preferred orientation. For flat specimens, back pressing and side drifting into the sample holder can be effective. These methods tend to produce much less preferred orientation than front-mounted samples, but tend not to be very effective for chronic preferred orientation such as that exhibited by phases like clays, feldspars and chlorite. Reducing the size of the crystallites improves the probability of achieving random alignment of the crystallites in the sample holder. Gradually milling a sample and monitoring the preferred-orientation coefficients as a function of grinding time may again help to find the correct, or at least reproducible, grinding conditions (Fig. 3.9.18).

A major advantage of whole-pattern-based QPA over single-peak methods is that all classes of reflections are considered in the calculation. In this sense, the method is less prone to preferred orientation of a particular class of peaks. Furthermore, orientation effects may be corrected by applying March–Dollase (Dollase, 1986) or spherical-harmonics (Ahtee *et al.*, 1989) corrections. A properly applied correction may be of high importance for QPA in cases where a phase is present at low concentration and only a few peaks can clearly be identified in the pattern. If those peak(s) are affected by preferred orientation, the March–Dollase coefficient correlates strongly with scale factors and leads to biased QPA results. Examples of this effect occur with layered materials that have sheet-like morphology perpendicular to the *c* axis, including mica and clay minerals, which typically show stronger than expected intensity for the 00*l* reflections.

The crucial factor seems to be to what extent the orientation parameters correlate with the Rietveld scale factor. An example where the correlation is only minor is sample 2 from the IUCr CPD round robin on QPA (Scarlett *et al.*, 2002). In that example, brucite [$Mg(OH)_2$] shows strong preferred orientation along the 00*l* direction. This may be corrected by the March–Dollase model, which returns a refined value of 0.66. However, the introduction of this preferred-orientation correction only changes the brucite concentration from 35 to 36 wt% (weighed = 36.36 wt%); this is surprising because the orientation is strong and the weighted residual R_{wp} changes from 30 to 15%. Close examination of the correlations reveals a strong correlation between the brucite scale factor and preferred-orientation factor.

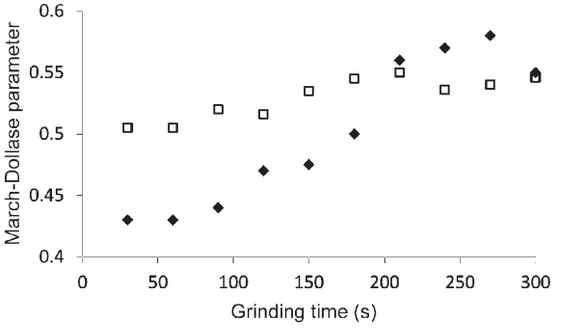

Figure 3.9.18
Increase of the March–Dollase (Dollase, 1986) parameter and related decrease of the degree of preferred orientation with grinding time for the two amphibole species actinolite (filled diamonds) and grunerite (open squares) in an iron ore. Data courtesy ThyssenKrupp – Resource Technologies (Knorr & Bornefeld, 2013).

However, the correlation of the brucite preferred-orientation parameter to the other scale factors (zincite, corundum and fluorite) is close to zero; this explains why in this example the QPA is not highly dependent on preferred orientation. In cases of strong correlation between the orientation parameter of one phase and the scale factors of other phases, preferred orientation should probably not be refined, or at least it should be verified carefully. It is worth noting that, in all Rietveld-based analyses, users should examine the correlation matrix as a matter of general practice to establish which parameters might be affecting parameters of interest.

It should be noted that sample rotation around the scattering vector (typically employed in flat-plate Bragg–Brentano geometry) during the scan does not reduce preferred orientation, since there is no change between the preferred-orientation direction and the diffraction vector. Using capillaries in transmission geometry assists in the reduction of preferred orientation, but the time-consuming nature of packing capillaries makes this technique infeasible in industrial applications where diffraction-based QPA is used for routine quality control.

3.9.10.3.3. *Microabsorption*

The strongest on-going impediment to accuracy in QPA using XRD data is microabsorption. The microabsorption effect occurs when a multiphase sample contains both low- and highly absorbing phases. For the highly absorbing phases, the X-ray beam is more likely to be absorbed in the surface layers of the grain; thus, the fraction of the grain contributing to the diffraction pattern will decrease as the size of the grain increases above the beam-penetration depth. For the low-absorbing phases, the beam penetrates further into the particle resulting in a greater likelihood of the desired 'volume diffraction' occurring (Brindley, 1945). The overall effect is the observation of a disproportionate amount of observed intensity from individual grains relative to what would be expected for the average absorption of the sample; the highly absorbing phases are under-represented relative to the low-absorbing phases. There is extensive discussion of the microabsorption issue in Zevin & Kimmel (1995).

Brindley (1945) has described the particle absorption contrast factor τ_α as

$$\tau_\alpha = (1/V)\int_0^V \exp\left(-(\mu_\alpha - \bar{\mu})\right) \mathrm{d}v, \qquad (3.9.48)$$

where V is the particle volume, and μ_α and $\bar{\mu}$ are the linear absorption coefficients of phase α and the entire sample, respectively. While it is relatively easy to calculate the absorption coefficients, equation (3.9.48) implies knowledge of the *particle* size of each component; this information is only available through independent microscope or light-scattering characterization.

This correction term is commonly incorporated into QPA through a modification to equation (3.9.26) of the form

$$W_\alpha = \frac{S_\alpha (ZMV)_\alpha / \tau_\alpha}{\sum_{k=1}^{n} S_k (ZMV)_k / \tau_k}. \qquad (3.9.49)$$

Brindley has also devised criteria by which to assess whether a microabsorption problem is likely to be present or not. Calculation of μD (where μ is the linear absorption coefficient and D is the particle diameter) yields the following criteria:

(i) $\mu D < 0.01$ – fine powder. There is negligible microabsorption and hence no correction is necessary.

Table 3.9.5
Calculated values of μD (where μ is the linear absorption coefficient and D is the particle diameter) for Cu $K\alpha$ X-rays for corundum, magnetite and zircon with a range of particle sizes

	μD		
Diameter (μm)	Corundum, Al_2O_3 (μ = 125 cm^{-1})	Magnetite, Fe_3O_4 (μ = 1167 cm^{-1})	Zircon, $ZrSiO_4$ (μ = 380 cm^{-1})
0.1	0.001	0.012	0.004
0.2	0.003	0.023	0.008
0.5	0.006	0.058	0.019
1	0.013	0.117	0.038
2	0.025	0.233	0.076
5	0.063	0.584	0.190
10	0.125	1.167	0.380
20	0.251	2.334	0.759

(ii) $0.01 < \mu D < 0.1$ – medium powder. Microabsorption is likely to be present and the normal Brindley correction model can be applied.

(iii) $0.1 < \mu D < 1.0$ – coarse powder. A large microabsorption effect is present. The Brindley model can only be used to provide an approximate correction provided that μD is closer to the lower limit of the range.

(iv) $\mu D > 1.0$ – very coarse powder. This indicates that severe microabsorption is likely to be present and that any correction is well beyond the limits of the model.

It is difficult for the analyst encountering a new sample to determine whether a correction for microabsorption is required without first obtaining additional information. A minimum requirement should be to calculate μD for each phase present. However, this requires knowledge of the particle size which, in a multiphase sample, can be very difficult to obtain unambiguously. Even when the particle size is measured by, for example, dynamic light scattering or optical or SEM image analysis, the applicability of the correction can still be unclear. In addition, the correction factor embodied in equations (3.9.48) and (3.9.49) makes the assumption that the particles of the phase of interest are spherical and of uniform size. This assumption is unrealistic in almost all samples; in reality, each phase is likely to be present at a wide range of particle sizes and the particles are highly unlikely to be spherical.

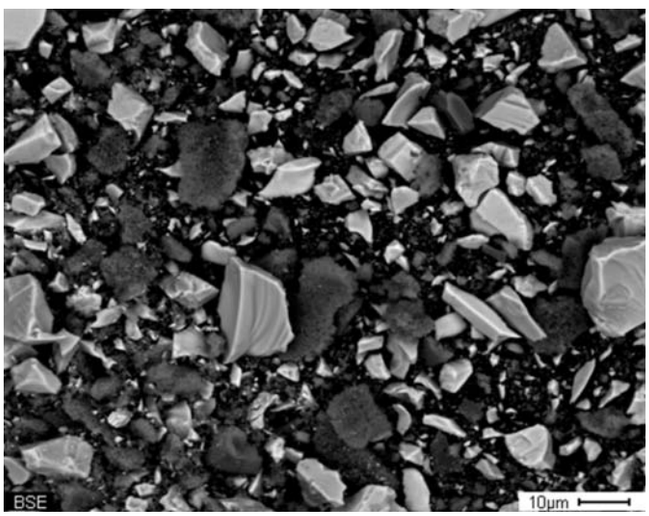

Figure 3.9.19
Backscattered-electron SEM image of a mixture of approximately equal amounts of corundum (dark grey), magnetite and zircon (lighter grey). Note the wide range of particle sizes present for each of the three phases.

Table 3.9.5 shows the calculated values of μD for Cu $K\alpha$ radiation for some commonly encountered phases in mineralogical analysis. For the least absorbing phase (corundum), the upper range of applicability of the Brindley model (medium powder) is reached at about 5 μm; by 8 μm, the coarse powder criterion has been reached and the correction model is no longer applicable. For magnetite, these limits are reached an order of magnitude earlier at about 0.5 and 0.9 μm, respectively.

Fig. 3.9.19 shows an SEM image of a mixture of approximately equal amounts of corundum, magnetite and zircon. The individual components of the sample were weighed and the mixture ground in ethanol in a McCrone micronizing mill (McCrone Research Associates, London) for 10 min g^{-1}. This approach to sample preparation is generally accepted as best practice for powder XRD because it minimizes structural damage during grinding (Hill & Madsen, 2002). After decanting and drying, the sample was back-packed into a cavity sample holder for XRD data collection; the same sample was then used to obtain the SEM image in Fig. 3.9.19. Visual observation shows a wide range of particle sizes (from submicron to greater than 10 μm) and shapes that do not even approximate spheres. Even if this information is obtained, selection of a particle size that best represents each individual phase is a difficult task. In addition, in many sample suites, the component phases exhibit a range of hardness resulting in different rates of grinding and hence difference size ranges. Regrettably, what happens too often in practice is that analysts will micronize the sample and then select an arbitrary particle size in order to derive a 'preferred' value for the final analysis. Therefore, caution is advised in the application of these correction models. The IUCr CPD round robin on QPA (Madsen *et al.*, 2001; Scarlett *et al.*, 2002) showed that many participants severely degraded their results by applying a correction when none was necessary.

Equation (3.9.48) shows that there two ways to minimize microabsorption. The first is to reduce the absorption contrast by, for example, changing the X-ray wavelength. While corundum and magnetite have very different linear absorption coefficients for Cu $K\alpha$ radiation (126 and 1123 cm^{-1}, respectively), the difference is reduced to 196 and 231 cm^{-1}, respectively, for Co $K\alpha$ radiation. The second approach is to reduce the particle size in order to meet Brindley's fine- or medium-powder criteria.

However, even these steps may not be sufficient to eliminate the microabsorption effect. Slightly different absorption coefficients, or different particle sizes for phases with the same absorption coefficients, may still introduce a bias between expected and analysed concentrations. In this situation, it may be better to use a calibrated hkl_phase or peaks_phase (Section 3.9.6) instead of a Rietveld, structure-based phase. The calibration step involved in the generation of such a phase incorporates the microabsorption problem into the calibration constant.

Fig. 3.9.20 shows the bias between known concentrations (derived from chemical analysis) and QPA-determined concentrations for a series of salt samples. The samples contain halite (NaCl), sylvite (KCl) and kieserite ($MgSO_4{\cdot}H_2O$) as major phases and small amounts of anhydrite ($CaSO_4$), langbeinite [$K_2Mg_2(SO_4)_3$] and carnallite [$KMgCl_3{\cdot}6(H_2O)$]. The linear absorption coefficient of sylvite (254 cm^{-1}) is much higher than halite (165 cm^{-1}). Using crystal-structure-based analysis, there is a systematic deviation of up to 3% with an overestimation of the low absorber (halite) and an underestimation of the high absorber (sylvite). After replacing sylvite by a calibrated

hkl_phase, the bias is reduced to about 1% and does not show systematic deviations.

It should be noted, however, that the phase constants developed using such a calibration approach will only be applicable to the sample suite and preparation conditions for which it was developed. The calibration process will need to be repeated if there are significant changes to the sample suite or sample-preparation conditions.

3.9.10.3.4. *Whole-pattern-refinement effects*

One of the distinct advantages of structure-based whole-pattern fitting for QPA is that no standards need to be prepared because the structure for each phase provides the phase constant *ZMV*; the unit-cell dimensions allow the calculation of the cell volume *V* and the unit-cell contents provide the mass *ZM* (Bish & Howard, 1988; Hill & Howard, 1987). These values are used, along with the Rietveld scale factor *S*, in equation (3.9.26) to derive the phase abundance. This is especially useful for complex systems where the preparation of multiple standards would add considerably to the analytical complexity.

An additional advantage is the ability to refine the crystal structure (unit-cell dimensions and site-occupation factors, for example), when the data are of sufficiently high quality, in order to obtain the best fit between observed and calculated patterns. In addition to updating the *ZMV* value, the site occupancies are contained in the structure-factor calculation and, therefore, will change the relative reflection intensities and have an impact on the scale factor and QPA. Other structural parameters that have a strong effect on the scale factor and QPA are the atomic displacement parameters (ADPs). Strong correlation between the ADPs and amorphous material concentration has been shown by Gualtieri (2000) and Madsen *et al.* (2011).

This leads to the question: which crystal structure should be selected for QPA? Databases contain multiple entries for the same phase with the structures determined using different methods. While ADPs and site-occupation factors determined using neutron diffraction and single-crystal analysis should be favoured over those determined using X-ray powder data, many database entries do not have refined ADPs for all (and in some cases, any) atoms. Often, arbitrarily chosen default values of 0.5 or 1.0 $Å^2$ for B_{eq} are entered for all atoms, but this should be viewed or used with great caution. There is clearly a need to carefully evaluate the crystal-structure data used for QPA. This is particularly worth mentioning in view of the advent of new 'user-friendly' software that automatically assigns crystal structures after having performed the phase identification.

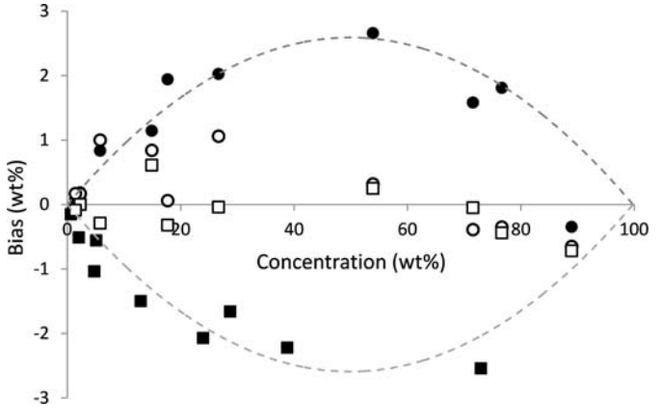

Figure 3.9.20
Bias as a function of phase concentration for industrial salt samples for (i) structure-based QPA (filled symbols) and (ii) calibrated hkl_phase (open symbols) for halite (circles) and sylvite (squares). The broken lines indicate the trend of the bias for structure-based QPA. Data are courtesy of K+S AG, Germany.

Empirical profile-shape models contribute significantly to the complexity (and correlations) of whole-powder-pattern fitting for QPA because of the large number of phases and multiple parameters required to model the profile shape of each phase. The use of convolution-based profile fitting [in, for example, *BGMN* (Bergmann *et al.*, 1998, 2000) and *TOPAS* (Bruker AXS, 2013)] greatly reduces the number of parameters, because the instrument-resolution function (which is constant for a given setup) can be separated from sample-related peak broadening. The instrument component can be refined using a standard and then fixed for subsequent analysis. The sample contribution to peak width and shape can then be related directly to crystallite size and microstrain using a minimal number of parameters. The reduction of the total number of parameters reduces the refinement complexity and the chance of parameter correlation.

The choice of the function used to model the pattern background may also have a strong influence on amorphous content (Gualtieri, 2000; Madsen *et al.*, 2011). Given that the intensities of both the background and the amorphous contribution vary slowly as a function of 2θ, it is inevitable that there will be a high degree of correlation between them. Hence, any errors in determining the true background will result in errors in amorphous phase determination. A simple approach is to use a background function with a minimal number of parameters. A more exact approach requires the separation of the amorphous contribution from background components such as Compton scattering and parasitic scattering by the sample environment and air in the beam path. This is routinely done in pair distribution function (PDF) analysis; details can be found in Chapter 5.7 in this volume and in Egami & Billinge (2003).

Another parameter that correlates with the pattern background is the width of broad peaks for phases of low concentration. If allowed to refine to very large width values, the peaks are 'smeared' over a broad range of the pattern with no clear distinction between peaks and background. The same issue applies when there is a high degree of peak overlap, particularly at high angles, leading to severe under- or over-estimation of the phase. The careful use of limits for either crystallite size or corresponding parameters in empirical peak-shape modelling assists in minimizing this effect.

There can be a subtle interplay between the profile-shape function and the pattern background that has an impact on whole-pattern fitting (Hill, 1992). The data in Fig. 3.9.21, collected using a Cu tube and an Ni $K\beta$ filter, exhibit low-angle truncation of the peak tails at the β-filter absorption edge. On the high-angle side, the anatase peak displays a wide tail which extends to the position of the strongest rutile peak at about 27.5° 2θ. In this case, rutile is present as a minor phase and the error in the background determination using conventional peak-profile modelling (Fig. 3.9.21*a*) introduces about 0.5% bias in the rutile QPA. The use of a more accurate profile model that incorporates the effect of the β-filter absorption edge (Fig. 3.9.21*b*) serves to improve the accuracy (Bruker AXS, 2013).

3.9.10.3.5. *Element analytical standards*

XRD-based derivation of elemental abundances relies on (i) the QPA abundances, and (ii) the assumed or measured stoichiometry of the crystalline phases. The accuracy of the QPA

Table 3.9.6
Compositional analysis of the Dillinger Hütte iron-ore certified reference material SX 11-14, (i) derived from QPA results, taking into account the nominal stoichiometry of the phases (XRD) and (ii) the certified analyses (Cert) (Knorr & Bornefeld, 2013)

Phase	wt%		Fe	FeO	SiO_2	Al_2O_3	MgO	CaO	K_2O	Na_2O	C
Haematite	0.37		0.26	—	—	—	—	—	—	—	—
Goethite	3.86		2.43	—	—	—	—	—	—	—	—
Magnetite	85.97		62.21	26.68	—	—	—	—	—	—	—
Quartz	5.73		—	—	5.73	—	—	—	—	—	—
Gibbsite	0.71		—	—	—	0.46	—	—	—	—	—
Talc	1.79		—	—	1.13	—	0.57	—	—	—	—
Orthoclase	0.30		—	—	0.19	0.05	—	—	0.05	—	—
Albite	0.89		—	—	0.60	0.18	—	—	—	0.10	—
Calcite	0.40		—	—	—	—	—	0.22	—	—	0.19
			Fe	FeO	SiO_2	Al_2O_3	MgO	CaO	K_2O	Na_2O	C
		XRD	64.89	26.68	7.66	0.70	0.57	0.22	0.05	0.10	0.19
		Cert	65.55	27.20	7.47	0.27	0.56	0.42	0.06	0.08	0.12
		Bias	−0.66	−0.52	0.19	0.43	0.01	−0.20	−0.01	0.02	0.07

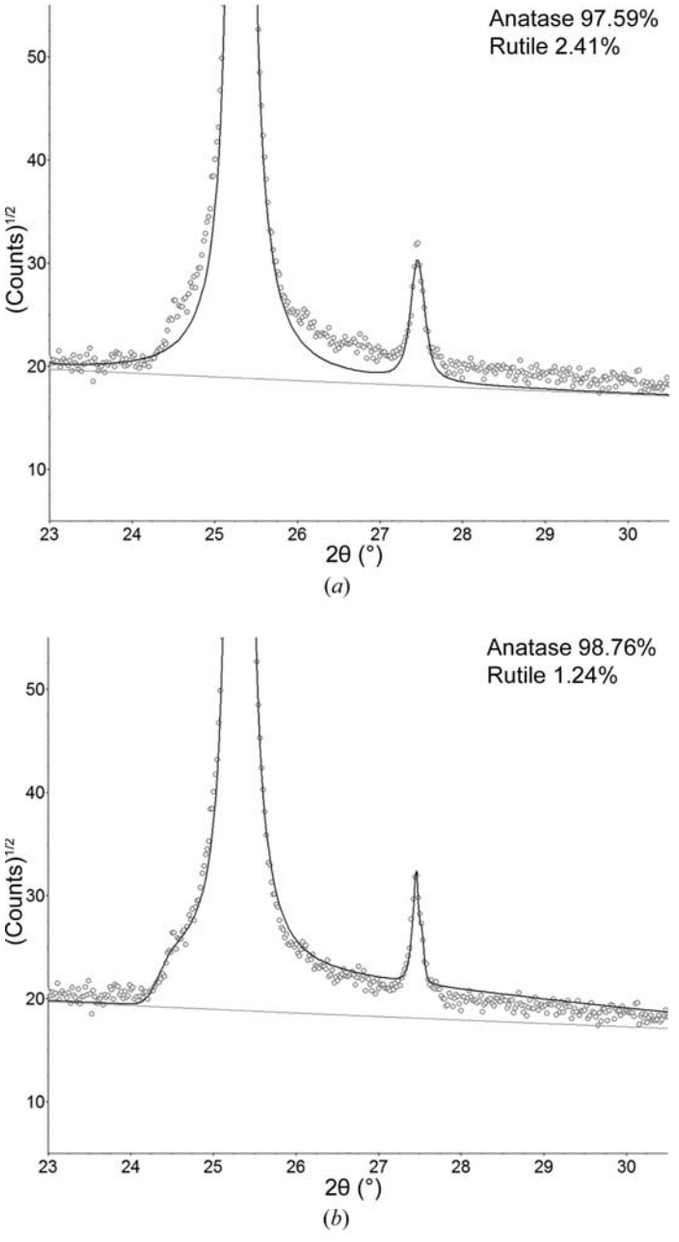

Figure 3.9.21
Profile fit of anatase and rutile (*a*) without and (*b*) with a $K\beta$ filter absorption-edge correction.

result may then be evaluated by comparing the calculated elemental abundances with those determined by traditional chemical-analysis techniques. However, for the best level of agreement, this method requires that the composition of the crystalline phases be well defined. A complication, in particular for minerals, is that idealized compositions may be reported but do not necessarily match the actual composition of the species present in the sample. Where possible, detailed phase analysis using microbeam techniques should be undertaken to establish the true composition for each phase. A complication that serves to decrease the agreement is that chemically based compositional analysis does not distinguish between crystalline and amorphous phase content, while the diffraction-based QPA usually measures only the crystalline phases. Generally, the composition of amorphous phases may not be known accurately and even highly crystalline material can contain amorphous components because of non-diffracting surface layers of the grains (Cline *et al.*, 2011).

An example demonstrating the level of agreement that can be achieved is that of the iron-ore certified reference material SX 11-14 from Dillinger Hütte (Fig. 3.9.22). The material is moderately complex and consists of nine distinct mineral species. The data were measured with Co $K\alpha$ radiation and analysed using Rietveld-based QPA in *TOPAS* (Bruker AXS, 2013). The phase abundances are converted to elemental and oxide compositions for comparison with the certified elemental analyses (Table 3.9.6). There is excellent agreement between the XRD results and the chemical analysis with bias values better than ±1 wt%.

3.9.10.3.6. *Phase-specific methods: diffraction SRMs, round-robin samples and synthetic mixtures*

In contrast to elemental compositional analysis, where standard reference materials (SRMs) are widespread, there are only a very limited number of SRMs available for diffraction-based QPA. Prominent examples are SRMs for the cement industry [NIST reference material clinker 8486 (Stutzman & Leigh, 2000) and ordinary Portland cement NIST SRM 2686] or ceramics materials (silicon nitride CRM BAM-S001) (Peplinski *et al.*, 2004). Similar to elemental standards, the certified values do not necessarily represent the true composition. Rather, they are published values that are typically averaged over the results from different independent methods, instruments and laboratories. Therefore, confidence limits of concentrations are provided that may be much larger than estimated standard deviations of concentrations within a single laboratory.

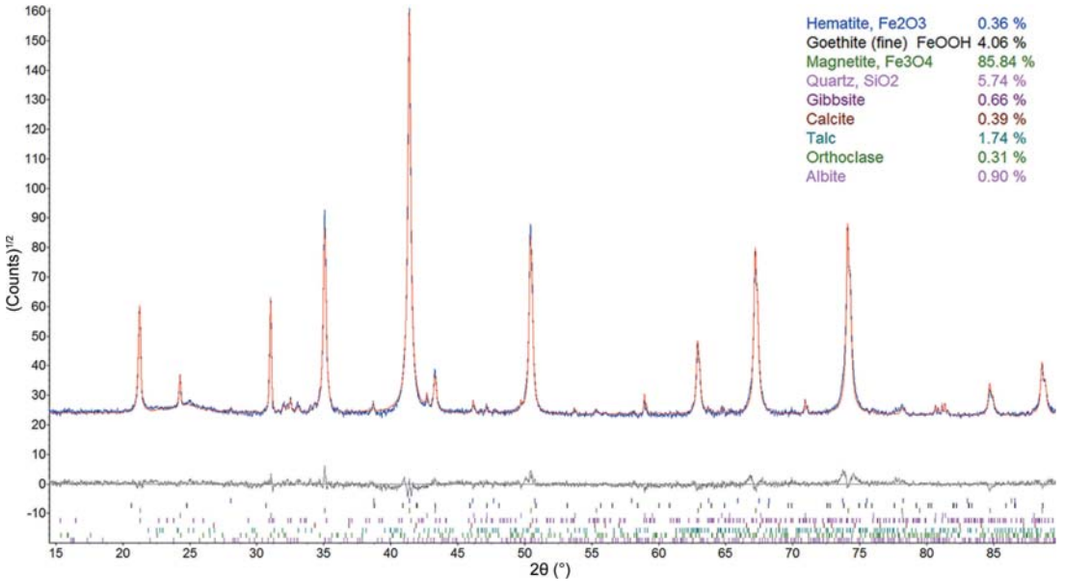

Figure 3.9.22
Output of Rietveld refinement and results of QPA for the iron-ore certified reference material SX 11-14 from Dillinger Hütte. The data were measured with Co *Kα* radiation.

Finally, a number of inter-laboratory tests, or round robins, have been conducted on synthetic mixtures in order to set benchmarks for particular materials and/or the application of methods. Examples range from well ordered, high-symmetry phases discussed in earlier sections of this chapter (Madsen *et al.*, 2001; Scarlett *et al.*, 2002) to standard mixtures of geological material, granite and bauxites (Bish & Post, 1993), and technical products like artificial Portland cements (De la Torre & Aranda, 2003) where relative biases of 2–3% for the main phases and 5–10% for minor phases were found.

Very recently, the precision and accuracy of QPA for the analysis of Portland clinker and cement were determined for synthetic mixtures and commercial samples. The scatter of the results from the inter-laboratory comparison, and the fact that individual errors are much smaller than the standard deviations of all submitted results, points to the widespread presence of user-dependent systematic errors (Léon-Reina *et al.*, 2009).

One of the most challenging round robins is the Reynolds Cup (Ottner *et al.*, 2000; McCarty, 2002; Kleeberg, 2005; Omotoso *et al.*, 2006; Raven & Self, 2017), organized biannually since the year 2000 by the Clay Minerals Society. Synthetic mixtures representing typical sedimentary rock types are analysed and require a very high level of sample preparation and analytical skills because of the presence of a variety of clay minerals.

While most round robins have dealt with inorganic materials, one for pharmaceutical materials was organised by the International Centre for Diffraction Data (ICDD) together with the Pharmaceutical Powder XRD symposium series (PPXRD) (Fawcett *et al.*, 2010). A major outcome was the identification of operator errors in all steps of the analysis to be the largest source of error. This highlights the importance of reducing systematic errors for improving accuracy in QPA.

As a concluding remark, a variety of factors may influence the precision and accuracy of QPA. Nonetheless, better than 1 wt% agreement may be achieved for simple systems of well crystallized material. Moderately complex mixtures such as those routinely observed in cement plants and in the mining industry can be typically analysed at a 1 wt% level of accuracy provided that the analyst chooses the most appropriate sample-preparation, data-collection and analysis methodologies for the samples in question.

3.9.11. Summary

The value in using diffraction-based methods for the determination of phase abundance arises from the fact that the observed data are derived directly from the crystal structure of each phase. Knowledge of phase abundance is valuable in many fields including (i) mineral exploration, where the type and amount of major minerals serve as indicators for valuable minor minerals, (ii) mineral extraction, where the performance of the process line is governed by the mineralogy, not the commonly used elemental compositions, (iii) *in situ* studies, where the mechanism and kinetics of phase evolution resulting from the application of an external variable can be examined and (iv) the optimization of production conditions for advanced materials.

The methodology of QPA is fraught with difficulties, many of which are experimental or derive from sample-related issues. Hence, it is necessary to verify diffraction-based phase abundances against independent methods. This should include calculation of the expected sample element composition (using the QPA and an assumed or measured composition of each phase) and comparing these values with the measured element composition. In those circumstances where this is not possible, the QPA values should be regarded only as semi-quantitative. While such values may be useful for deriving trends within a particular system, they cannot be regarded as an absolute measure.

References

Ahtee, M., Nurmela, M., Suortti, P. & Järvinen, M. (1989). *Correction for preferred orientation in Rietveld refinement. J. Appl. Cryst.* **22**, 261–268.

Alexander, L. E. & Klug, H. P. (1948). *Basic aspects of X-ray absorption in quantitative diffraction analysis of powder mixtures. Anal. Chem.* **20**, 886–889.

Ballirano, P. & Caminiti, R. (2001). *Rietveld refinements on laboratory energy dispersive X-ray diffraction (EDXD) data. J. Appl. Cryst.* **34**, 757–762.

Barnes, P., Colston, S., Craster, B., Hall, C., Jupe, A., Jacques, S., Cockcroft, J., Morgan, S., Johnson, M., O'Connor, D. & Bellotto, M.

(2000). *Time- and space-resolved dynamic studies on ceramic and cementitious materials. J. Synchrotron Rad.* **7**, 167–177.
Batchelder, M. & Cressey, G. (1998). *Rapid, accurate phase quantification of clay-bearing samples using a position-sensitive X-ray detector*. *Clays Clay Miner.* **46**, 183–194.
Bergmann, J., Friedel, P. & Kleeberg, R. (1998). *Bgmn – a new fundamental parameters based Rietveld program for laboratory X-ray sources; its use in quantitative analysis and structure investigations*. *IUCr Commission on Powder Diffraction Newsletter*, **20**, 5–8.
Bergmann, J. & Kleeberg, R. (1998). *Rietveld analysis of disordered layer silicates. Mater. Sci. Forum*, **278–281**, 300–305.
Bergmann, J., Kleeberg, R., Haase, A. & Breidenstein, B. (2000). *Advanced fundamental parameters model for improved profile analysis. Mater. Sci. Forum*, **347–349**, 303–308.
Bette, S., Dinnebier, R. E. & Freyer, D. (2015). *Structure solution and refinement of stacking-faulted NiCl(OH). J. Appl. Cryst.* **48**, 1706–1718.
Bish, D. L. & Howard, S. A. (1988). *Quantitative phase analysis using the Rietveld method. J. Appl. Cryst.* **21**, 86–91.
Bish, D. L. & Post, J. E. (1993). *Quantitative mineralogical analysis using the Rietveld full-pattern fitting method. Am. Mineral.* **78**, 932–940.
Bogue, R. H. (1929). *Calculation of the compounds in Portland cement. Ind. Eng. Chem. Anal. Ed.* **1**, 192–197.
Bordas, J., Glazer, A. M., Howard, C. J. & Bourdillon, A. J. (1977). *Energy-dispersive diffraction from polycrystalline materials using synchrotron radiation. Philos. Mag.* **35**, 311–323.
Brindley, G. W. (1945). *The effect of grain or particle size on X-ray reflections from mixed powders and alloys, considered in relation to the quantitative determination of crystalline substances by X-ray methods. London Edinb. Dubl. Philos. Mag. J. Sci.* **36**, 347–369.
Brindley, G. W. (1980). *Crystal structures of clay minerals and their X-ray identification*. Mineralogical Society Monograph No. 5, edited by G. W. Brindley & G. Brown, pp. 125–195. London: Mineralogical Society.
Bruker AXS (2013). *Topas v5: General profile and structure analysis software for powder diffraction data*. Version 5. https://www.bruker.com/topas.
Buhrke, V. E., Jenkins, R. & Smith, D. K. (1998). *A Practical Guide for the Preparation of Specimens for X-Ray Fluorescence and X-ray Diffraction Analysis*. New York: Wiley-VCH.
Buras, B., Gerward, L., Glazer, A. M., Hidaka, M. & Staun Olsen, J. (1979). *Quantitative structural studies by means of the energy-dispersive method with X-rays from a storage ring. J. Appl. Cryst.* **12**, 531–536.
Casas-Cabanas, M., Rodríguez-Carvajal, J. & Palacín, M. R. (2006). *FAULTS, a new program for refinement of powder diffraction patterns from layered structures. Z. Kristallogr. Suppl.* **23**, 243–248.
Cernik, R. J., Hansson, C. C. T., Martin, C. M., Preuss, M., Attallah, M., Korsunsky, A. M., Belnoue, J. P., Jun, T. S., Barnes, P., Jacques, S., Sochi, T. & Lazzari, O. (2011). *A synchrotron tomographic energy-dispersive diffraction imaging study of the aerospace alloy Ti 6246. J. Appl. Cryst.* **44**, 150–157.
Cheary, R. W. & Coelho, A. (1992). *A fundamental parameters approach to X-ray line-profile fitting. J. Appl. Cryst.* **25**, 109–121.
Cheary, R. W., Coelho, A. A. & Cline, J. P. (2004). *Fundamental parameters line profile fitting in laboratory diffractometers. J. Res. Natl Inst. Stand. Technol.* **109**, 1–25.
Chipera, S. J. & Bish, D. L. (2002). *FULLPAT: a full-pattern quantitative analysis program for X-ray powder diffraction using measured and calculated patterns. J. Appl. Cryst.* **35**, 744–749.
Chipera, S. J. & Bish, D. L. (2013). *Fitting full X-ray diffraction patterns for quantitative analysis: a method for readily quantifying crystalline and disordered phases. Adv. Mater. Phys. Chem.* **3**, 47–53.
Chung, F. H. (1974*a*). *Quantitative interpretation of X-ray diffraction patterns of mixtures. I. Matrix-flushing method for quantitative multicomponent analysis. J. Appl. Cryst.* **7**, 519–525.
Chung, F. H. (1974*b*). *Quantitative interpretation of X-ray diffraction patterns of mixtures. II. Adiabatic principle of X-ray diffraction analysis of mixtures. J. Appl. Cryst.* **7**, 526–531.
Chung, F. H. & Smith, D. K. (2000). *Industrial Applications of X-ray Diffraction*, edited by F. H. Chung & D. K. Smith, ch. 1, pp. 3–10, and ch. 2, pp. 13–32. New York: Marcel Dekker.
Cline, J. P., Von Dreele, R. B., Winburn, R., Stephens, P. W. & Filliben, J. J. (2011). *Addressing the amorphous content issue in quantitative phase analysis: the certification of NIST standard reference material 676a. Acta Cryst.* A**67**, 357–367.
Coelho, A. A., Evans, J. S. O. & Lewis, J. W. (2016). *Averaging the intensity of many-layered structures for accurate stacking-fault analysis using Rietveld refinement. J. Appl. Cryst.* **49**, 1740–1749.
Coelho, A. A., Chater, P. A. and Kern, A. (2015). *Fast synthesis and refinement of the atomic pair distribution function. J. Appl. Cryst.* **48**, 869–875
Cowley, J. M. (1976). *Diffraction by crystals with planar faults. I. General theory. Acta Cryst.* A**32**, 83–87.
Cressey, G. & Schofield, P. F. (1996). *Rapid whole-pattern profile-stripping method for the quantification of multiphase samples. Powder Diffr.* **11**, 35–39.
De La Torre, A. G., Ángeles, G., Bruque, S., Campo, J. & Aranda, M. A. G. (2002). *The superstructure of C3S from synchrotron and neutron powder diffraction and its role in quantitative phase analyses. Cem. Concr. Res.* **32**, 1347–1356.
De la Torre, A. G. & Aranda, M. A. G. (2003). *Accuracy in Rietveld quantitative phase analysis of Portland cements. J. Appl. Cryst.* **36**, 1169–1176.
Debye, P. & Scherrer, P. (1916). *Interferenzen an regellos orientierten Teilchen im Röntgenlicht Phys. Z.* **17**, 277–283.
Debye, P. & Scherrer, P. (1917). *X-ray interference produced by irregularly oriented particles: Constitution of graphite and amorphous C. Phys. Z.* **18**, 291–301.
Dohrmann, R., Rüping, K. B., Kleber, M., Ufer, K. & Jahn, R. (2009). *Variation of preferred orientation in oriented clay mounts as a result of sample preparation and composition. Clays Clay Miner.* **57**, 686–694.
Dollase, W. A. (1986). *Correction of intensities for preferred orientation in powder diffractometry: application of the March model. J. Appl. Cryst.* **19**, 267–272.
Drits, V. A. & Tchoubar, C. (1990). *X-ray diffraction by disordered lamellar structures: Theory and application to microdivided silicates and carbons*. Heidelberg: Springer Verlag.
Eberl, D. D. (2003). *User's guide to rockjock - a program for determining quantitative mineralogy from powder x-ray diffraction data.* U.S. Geological Survey Open-File Report 2003-78. http://pubs.er.usgs.gov/publication/ofr200378.
Egami, T. & Billinge, S. J. L. (2003). *Underneath the Bragg Peaks: Structural Analysis of Complex Materials*. Oxford: Elsevier.
Ehrenberg, H., Senyshyn, A., Hinterstein, M. & Fuess, H. (2013). *Modern Diffraction Methods*, edited by E. J. Mittemeijer & U. Welzel, pp. 491–517. Weinheim: Wiley-VCH Verlag GMBH & Co.
Elton, N. J. & Salt, P. D. (1996). *Particle statistics in quantitative X-ray diffractometry. Powder Diffr.* **11**, 218–229.
Fawcett, T. G., Kabekkodu, S. N., Blanton, J. R. & Blanton, T. N. (2017). *Chemical analysis by diffraction: the Powder Diffraction File. Powder Diffr.* 32, 63–71.
Fawcett, T. G., Needham, F., Faber, J. & Crowder, C. E. (2010). *International Centre for Diffraction Data round robin on quantitative Rietveld phase analysis of pharmaceuticals. Powder Diffr.* **25**, 60–67.
Frost, D. J. & Fei, Y. (1999). *Static compression of the hydrous magnesium silicate phase d to 30 GPa at room temperature. Phys. Chem. Miner.* **26**, 415–418.
Glazer, A. M., Hidaka, M. & Bordas, J. (1978). *Energy-dispersive powder profile refinement using synchrotron radiation. J. Appl. Cryst.* **11**, 165–172.
Gualtieri, A. F. (2000). *Accuracy of XRPD QPA using the combined Rietveld–RIR method. J. Appl. Cryst.* **33**, 267–278.
Gualtieri, A. F., Viani, A., Banchio, G. & Artioli, G. (2001). *Quantitative phase analysis of natural raw materials containing montmorillonite. Mater. Sci. Forum*, **378–381**, 702–709.
Hall, C., Barnes, P., Cockcroft, J. K., Colston, S. L., Häusermann, D., Jacques, S. D. M., Jupe, A. C. & Kunz, M. (1998). *Synchrotron energy-dispersive X-ray diffraction tomography. Nucl. Instrum. Methods Phys. Res. B*, **140**, 253–257.
Hall, C., Colston, S. L., Jupe, A. C., Jacques, S. D. M., Livingston, R., Ramadan, A. O. A., Amde, A. W. & Barnes, P. (2000). *Non-destructive tomographic energy-dispersive diffraction imaging of the interior of bulk concrete. Cem. Concr. Res.* **30**, 491–495.
Hendricks, S. & Teller, E. (1942). *X-ray interference in partially ordered layer lattices. J. Chem. Phys.* **10**, 147–167.
Hill, R. J. (1983). *Calculated X-ray powder diffraction data for phases encountered in lead/acid battery plates. J. Power Sources*, **9**, 55–71.
Hill, R. J. (1991). *Expanded use of the Rietveld method in studies of phase abundance in multiphase mixtures. Powder Diffr.* **6**, 74–77.

Hill, R. J. (1992). *The background in X-ray powder diffractograms: a case study of Rietveld analysis of minor phases using Ni-filtered and graphite-monochromated radiation. Powder Diffr.* **7**, 63–70.

Hill, R. J. & Howard, C. J. (1987). *Quantitative phase analysis from neutron powder diffraction data using the Rietveld method. J. Appl. Cryst.* **20**, 467–474.

Hill, R. J., Howard, C. J. & Reichert, B. E. (1991). *Quantitative phase abundance in Mg-PSZ by Rietveld analysis of neutron and X-ray diffraction data. Mater. Sci. Forum*, **34–36**, 159–163.

Hill, R. J. & Madsen, I. C. (2002). *Structure Determination from Powder Diffraction Data*, edited by W. David, K. Shankland, L. McCusker & C. Baerlocher, ch. 6, pp. 98–116. Oxford University Press.

Hubbard, C. R., Evans, E. H. & Smith, D. K. (1976). *The reference intensity ratio, I/Ic, for computer simulated powder patterns. J. Appl. Cryst.* **9**, 169–174.

Hubbard, C. R. & Snyder, R. L. (1988). *RIR – measurement and use in quantitative XRD. Powder Diffr.* **3**, 74–77.

Hull, A. W. (1917). *A new method of X-ray crystal analysis. Phys. Rev*. **10**, 661–696.

Hull, A. W. (1919). *A new method of chemical analysis. J. Am. Chem. Soc.* **41**, 1168–1175.

ICDD (2015). The Powder Diffraction File, database of the International Centre for Diffraction Data, release PDF4+, 2015. ICDD, 12 Campus Boulevard, Newton Square, Pennsylvania 19073–3273, USA.

Kaduk, J. A. (2000). In *Industrial Applications of X-ray Diffraction*, edited by F. H. Chung & D. K. Smith, pp. 207–253. New York: Marcel Dekker.

Kleeberg, R. (2005). *Results of the second Reynolds Cup contest in quantitative mineral analysis*. IUCr Commission on Powder Diffraction Newsletter, **30**, 22–26.

Klug, H. P. & Alexander, L. E. (1974). *X-ray Diffraction Procedures: For Polycrystalline and Amorphous Materials*. New York: Wiley.

Knorr, K. & Bornefeld, M. (2013). Proceedings of Process Mineralogy ’12, 7–9 November 2012. Cape Town, South Africa, pp. 651–652. http://www.proceedings.com/16755.html.

Knudsen, T. (1981). *Quantitative X-ray diffraction analysis with qualitative control of calibration samples. X-ray Spectrom.* **10**, 54–56.

Langford, J. I. (2004). In *Diffraction Analysis of the Microstructure of Materials*, edited by E. J. Mittemeijer & P. Scardi, pp. 3–11. Berlin: Springer-Verlag.

Larson, A. C. & Von Dreele, R. B. (2004). *General Structure Analysis System (GSAS)*. Report LAUR 86-748, Los Alamos National Laboratory, New Mexico, USA.

Le Bail, A., Duroy, H. & Fourquet, J. L. (1988). *Ab-initio structure determination of $LiSbWO_6$ by X-ray powder diffraction. Mater. Res. Bull.* **23**, 447–452.

Le Bail, A. & Jouanneaux, A. (1997). *A qualitative account for anisotropic broadening in whole-powder-diffraction-pattern fitting by second-rank tensors. J. Appl. Cryst.* **30**, 265–271.

León-Reina, L., De la Torre, A. G., Porras-Vázquez, J. M., Cruz, M., Ordonez, L. M., Alcobé, X., Gispert-Guirado, F., Larrañaga-Varga, A., Paul, M., Fuellmann, T., Schmidt, R. & Aranda, M. A. G. (2009). *Round robin on Rietveld quantitative phase analysis of Portland cements. J. Appl. Cryst.* **42**, 906–916.

Leoni, M., Gualtieri, A. F. & Roveri, N. (2004). *Simultaneous refinement of structure and microstructure of layered materials. J. Appl. Cryst.* **37**, 166–173.

Lippmann, F. (1970). *Functions describing preferred orientation in flat aggregates of flake-like clay minerals and in other axially symmetric fabrics. Contr. Miner. Petrol.* **25**, 77–94.

McCarty, D. K. (2002). *Quantitative mineral analysis of clay-bearing mixtures: The ‘Reynolds Cup’ contest*. IUCr Commission on Powder Diffraction Newsletter, **27** 12–16.

Madsen, I. C., Scarlett, N. V. Y., Cranswick, L. M. D. & Lwin, T. (2001). *Outcomes of the International Union of Crystallography Commission on Powder Diffraction Round Robin on Quantitative Phase Analysis: samples 1a to 1h. J. Appl. Cryst.* **34**, 409–426.

Madsen, I. C., Scarlett, N. V. Y. & Kern, A. (2011). *Description and survey of methodologies for the determination of amorphous content via x-ray powder diffraction. Z. Kristallogr.* **226**, 944–955.

Madsen, I. C., Scarlett, N. V. Y., Riley, D. P. & Raven, M. D. (2013). *Modern Powder Diffraction*, edited by E. J. Mittemeijer & U. Welzel, pp. 283–320. Weinheim: Wiley-VCH.

Madsen, I. C., Scarlett, N. V. Y. & Whittington, B. I. (2005). *Pressure acid leaching of nickel laterite ores: an in situ diffraction study of the mechanism and rate of reaction. J. Appl. Cryst.* **38**, 927–933.

Michalski, E. (1988). *The diffraction of X-rays by close-packed polytypic crystals containing single stacking faults. I. General theory. Acta Cryst.* A**44**, 640–649.

Michalski, E., Kaczmarek, S. M. & Demianiuk, M. (1988). *The diffraction of X-rays by close-packed polytypic crystals containing single stacking faults. II. Theory for hexagonal and rhombohedral structures. Acta Cryst.* A**44**, 650–657.

Morris, R. E., Harrison, W. T. A., Nicol, J. M., Wilkinson, A. P. & Cheetham, A. K. (1992). *Determination of complex structures by combined neutron and synchrotron X-ray powder diffraction. Nature*, **359**, 519–522.

Murray, J., Kirwan, L., Loan, M. & Hodnett, B. K. (2009). *In-situ synchrotron diffraction study of the hydrothermal transformation of goethite to hematite in sodium aluminate solutions. Hydrometallurgy*, **95**, 239–246.

Navias, L. (1925). *Quantitative determination of the development of mullite in fired clays by an X-ray method. J. Am. Ceram. Soc.* **8**, 296–302.

Norby, P., Cahill, C., Koleda, C. & Parise, J. B. (1998). *A reaction cell for in situ studies of hydrothermal titration. J. Appl. Cryst.* **31**, 481–483.

O’Connor, B. H. & Raven, M. D. (1988). *Application of the Rietveld refinement procedure in assaying powdered mixtures. Powder Diffr.* **3**, 2–6.

Omotoso, O., McCarty, D. K., Hillier, S. & Kleeberg, R. (2006). *Some successful approaches to quantitative mineral analysis as revealed by the 3rd Reynolds Cup contest. Clays Clay Miner.* **54**, 748–760.

Ottner, F., Gier, S., Kuderna, M. & Schwaighofer, B. (2000). *Results of an inter-laboratory comparison of methods for quantitative clay analysis. Appl. Clay Sci.* **17**, 223–243.

Parrish, W. (1965). Editor. *X-ray Analysis Papers*, 2nd ed. Eindhoven: Centrex Publishing Company.

Pawley, G. S. (1980). *EDINP, the Edinburgh powder profile refinement program. J. Appl. Cryst.* **13**, 630–633.

Pawley, G. S. (1981). *Unit-cell refinement from powder diffraction scans. J. Appl. Cryst.* **14**, 357–361.

Peplinski, B., Kleeberg, R., Bergmann, J. & Wenzel, J. (2004). *Quantitative phase analysis using the Rietveld method – estimates of possible problems based on two interlaboratory comparisons. Mater. Sci. Forum*, **443-444**, 45–50.

Popa, N. C. (1998). *The (hkl) dependence of diffraction-line broadening caused by strain and size for all Laue groups in Rietveld refinement. J. Appl. Cryst.* **31**, 176–180.

Raven, M. D. & Self, P. G. (2017). *Outcomes of 12 years of the Reynolds Cup quantitative mineral analysis round robin. Clays Clay Miner.* **65**, 122–134.

Reynolds, R. C. (1985). *Newmod, a computer program for the calculation of one-dimensional diffraction patterns of mixed-layered clays.* Hanover, USA.

Reynolds, R. (1989). *Quantitative mineral analysis of clays*. In *CMS Workshop Lectures 1*, edited by D. R. Pevear & F. A. Mumpton, pp. 4–37. Boulder: The Clay Minerals Society.

Reynolds, R. C. (1994). *Wildfire, a computer program for the calculation of threee-dimensional powder X-ray diffraction patterns for mica polytypes and their disordered variations.* Hanover, USA.

Reynolds, R. C. & Hower, J. (1970). *The nature of interlayering in mixed-layer illite-montmorillonites. Clays Clay Miner.* **18**, 25–36.

Rietveld, H. M. (1969). *A profile refinement method for nuclear and magnetic structures. J. Appl. Cryst.* **2**, 65–71.

Rowles, M. R., Styles, M. J., Madsen, I. C., Scarlett, N. V. Y., McGregor, K., Riley, D. P., Snook, G. A., Urban, A. J., Connolley, T. & Reinhard, C. (2012). *Quantification of passivation layer growth in inert anodes for molten salt electrochemistry by in situ energy-dispersive diffraction. J. Appl. Cryst.* **45**, 28–37.

Scarlett, N. V. Y. & Madsen, I. C. (2006). *Quantification of phases with partial or no known crystal structures. Powder Diffr.* **21**, 278–284.

Scarlett, N. V. Y., Madsen, I. C., Cranswick, L. M. D., Lwin, T., Groleau, E., Stephenson, G., Aylmore, M. & Agron-Olshina, N. (2002). *Outcomes of the International Union of Crystallography Commission on Powder Diffraction Round Robin on Quantitative Phase Analysis: samples 2, 3, 4, synthetic bauxite, natural granodiorite and pharmaceuticals. J. Appl. Cryst.* **35**, 383–400.

Scarlett, N. V. Y., Madsen, I. C., Evans, J. S. O., Coelho, A. A., McGregor, K., Rowles, M., Lanyon, M. R. & Urban, A. J. (2009). *Energy-*

dispersive diffraction studies of inert anodes. *J. Appl. Cryst.* **42**, 502–512.

Scarlett, N. V. Y., Madsen, I. C., Pownceby, M. I. & Christensen, A. N. (2004). *In situ X-ray diffraction analysis of iron ore sinter phases*. *J. Appl. Cryst.* **37**, 362–368.

Scarlett, N. V. Y., Madsen, I. C. & Whittington, B. I. (2008). *Time-resolved diffraction studies into the pressure acid leaching of nickel laterite ores: a comparison of laboratory and synchrotron X-ray experiments*. *J. Appl. Cryst.* **41**, 572–583.

Scarlett, N. V. Y., Pownceby, M. I., Madsen, I. C. & Christensen, A. N. (2004). *Reaction sequences in the formation of silico-ferrites of calcium and aluminum in iron ore sinter*. *Metall. Mater. Trans. B*, **35**, 929–936.

Schmitt, B., Brönnimann, C., Eikenberry, E. F., Gozzo, F., Hörmann, C., Horisberger, R. & Patterson, B. (2003). *Mythen detector system*. *Nucl. Instrum. Methods Phys. Res. A*, **501**, 267–272.

Smith, D. K. (1992). *Particle statistics and whole pattern methods in quantitative x-ray powder diffraction analysis. Adv. X-ray Anal.* **35**, 1–15.

Smith, D. K., Johnson, G. G., Scheible, A., Wims, A. M., Johnson, J. L. & Ullmann, G. (1987). *Quantitative X-ray powder diffraction method using the full diffraction pattern*. *Powder Diffr.* **2**, 73–77.

Snyder, R. L. & Bish, D. L. (1989). In *Modern Powder Diffraction*, edited by D. L. Bish & J. E. Post, pp. 101–142. Washington DC: Mineralogical Society of America.

Stephens, P. W. (1999). *Phenomenological model of anisotropic peak broadening in powder diffraction*. *J. Appl. Cryst.* **32**, 281–289.

Stinton, G. W. & Evans, J. S. O. (2007). *Parametric Rietveld refinement*. *J. Appl. Cryst.* **40**, 87–95.

Stutzman, P. E. & Leigh, S. (2000). Proceedings of the Twenty-Second International Conference on Cement Microscopy, 11–13 September 2000, Quebec City, Canada. https://cemmicro.org/publications/.

Styles, M. J., Rowles, M. R., Madsen, I. C., McGregor, K., Urban, A. J., Snook, G. A., Scarlett, N. V. Y. & Riley, D. P. (2012). *A furnace and environmental cell for the in situ investigation of molten salt electrolysis using high-energy X-ray diffraction*. *J. Synchrotron Rad.* **19**, 39–47.

Taylor, J. C. (1991). *Computer programs for standardless quantitative analysis of minerals using the full powder diffraction profile*. *Powder Diffr.* **6**, 2–9.

Taylor, J. C. & Rui, Z. (1992). *Simultaneous use of observed and calculated standard profiles in quantitative XRD analysis of minerals by the multiphase Rietveld method: the determination of pseudorutile in mineral sands products*. *Powder Diffr.* **7**, 152–161.

Taylor, R. M. & Norrish, K. (1966). *The measurement of orientation distribution and its application to quantitative X-ray diffraction analysis*. *Clay Miner.* **6**, 127–142.

Toraya (2016*a*). *A new method for quantitative phase analysis using X-ray powder diffraction: direct derivation of weight fractions from observed integrated intensities and chemical compositions of individual phases. J. Appl. Cryst.* **49**, 1508–1516

Toraya (2016*b*). *A new method for quantitative phase analysis using X-ray powder diffraction: direct derivation of weight fractions from observed integrated intensities and chemical compositions of individual phases. Corrigendum. J. Appl. Cryst.* **50**, 665.

Toraya, H. & Tsusaka, S. (1995). *Quantitative phase analysis using the whole-powder-pattern decomposition method. I. Solution from knowledge of chemical compositions*. *J. Appl. Cryst.* **28**, 392–399.

Treacy, M. M. J., Newsam, J. M. & Deem, M. W. (1991). *A general recursion method for calculating diffracted intensities from crystals containing planar faults*. *Proc. R. Soc. London Ser. A*, **433**, 499–520.

Ufer, K., Kleeberg, R., Bergmann, J., Curtius, H. & Dohrmann, R. (2008). *Refining real structure parameters of disordered layer structures within the Rietveld method*. *Z. Kristallogr.* Suppl. **27**, 151–158.

Ufer, K., Kleeberg, R., Bergmann, J. & Dohrmann, R. (2012). *Rietveld refinement of disordered illite-smectite mixed-layer structures by a recursive algorithm. II: powder-pattern refinement and quantitative phase analysis*. *Clays Clay Miner.* **60**, 535–552.

Ufer, K., Roth, G., Kleeberg, R., Stanjek, H. & Dohrmann, R. (2004). *Description of x-ray powder pattern of turbostratically disordered layer structures with a Rietveld compatible approach*. *Z. Kristallogr.* **219**, 519–527.

Ufer, K., Stanjek, H., Roth, G., Dohrmann, R., Kleeberg, R. & Kaufhold, S. (2008). *Quantitative phase analysis of bentonites by the Rietveld method*. *Clays Clay Miner.* **56**, 272–282.

Wang, X., Li, J., Hart, R. D., van Riessen, A. & McDonald, R. (2011). *Quantitative X-ray diffraction phase analysis of poorly ordered nontronite clay in nickel laterites*. *J. Appl. Cryst.* **44**, 902–910.

Warren, B. E. (1941). *X-ray diffraction in random layer lattices*. *Phys. Rev.* **59**, 693–698.

Webster, N. A. S., Madsen, I. C., Loan, M. J., Knott, R. B., Naim, F., Wallwork, K. S. & Kimpton, J. A. (2010). *An investigation of goethite-seeded $Al(OH)_3$ precipitation using in situ X-ray diffraction and Rietveld-based quantitative phase analysis. J. Appl. Cryst.* **43**, 466–472.

Webster, N. A. S., Pownceby, M. I. & Madsen, I. C. (2013). *In situ X-ray diffraction investigation of the formation mechanisms of silico-ferrite of calcium and aluminium-I-type (SFCA-I-type) complex calcium ferrites*. *ISIJ Int.* **53**, 1334–1340.

Westphal, T., Füllmann, T. & Pöllmann, H. (2009). *Rietveld quantification of amorphous portions with an internal standard – mathematical consequences of the experimental approach*. *Powder Diffr.* **24**, 239–243.

Williams, R. P., Hart, R. D. & van Riessen, A. (2011). *Quantification of the extent of reaction of metakaolin-based geopolymers using X-ray diffraction, scanning electron microscopy, and energy-dispersive spectroscopy*. *J. Am. Ceram. Soc.* **94**, 2663–2670.

Yuan, H. & Bish, D. (2010). *NEWMOD+, a new version of the NEWMOD program for interpreting X-ray powder diffraction patterns from interstratified clay minerals*. *Clays Clay Miner.* **58**, 318–326.

Zevin, L. & Viaene, W. (1990). *Impact of clay particle orientation on quantitative clay diffractometry*. *Clay Miner.* **25**, 401–418.

Zevin, L. S. & Kimmel, G. (1995). *Quantitative X-ray Diffractometry*. Springer-Verlag New York, Inc.

Zhao, Y., Von Dreele, R. B., Shankland, T. J., Weidner, D. J., Zhang, J., Wang, Y. & Gasparik, T. (1997). *Thermoelastic equation of state of jadeite $NaAlSi_2O_6$: an energy-dispersive Rietveld refinement study of low symmetry and multiple phases diffraction*. *Geophys. Res. Lett.* **24**, 5–8.